BASIC AND APPLIED STUDIES OF CELL-MATRIX INTERACTIONS

A Dissertation

by

ABHISHEK TONDON

Submitted to the Office of Graduate and Professional Studies of
Texas A&M University
in partial fulfillment of the requirements for the degree of

DOCTOR OF PHILOSOPHY

Chair of Committee,	Roland R. Kaunas
Committee Members,	Kayla Bayless
	Carl Gregory
	Alvin T. Yeh
Head of Department,	Anthony Guiseppi-Elie

December 2015

Major Subject: Biomedical Engineering

ABSTRACT

Extracellular matrix is a complex network of molecules that accomplishes various roles within each tissue. The mechanical properties and biochemical composition of the extracellular matrix vary considerably across tissues. In addition to providing structural support and elasticity, extracellular matrix properties influence various cellular behavior and processes like adhesion, differentiation and proliferation, among others. In these studies, I focused on elucidating the effects of changes in matrix composition and stresses on cellular architecture. In addition, the insights gained from these studies were utilized to develop a novel cell-based disease model of Malignant Bone Disease in which human mesenchymal stem cells and bone tumor cells are co-cultured on osteogenic microsphere in a rotating wall vessel to promote the growth of 3D tissue constructs.

Successful execution of these studies will lead to a range of new methods for the investigation of tumor-stem cell interactions without the limitations of 2D tissue culture or in vivo approaches. Furthermore, we expect that this approach will significantly accelerate drug research and substantially improve our understanding of tumor expansion and bone repair during long term exposure to micro-gravity.

ACKNOWLEDGEMENTS

I am extremely grateful to my advisor, Professor Roland R. Kaunas, for his vital encouragement and guidance throughout my graduate studies and research. His patience and enthusiasm in research had motivated me. In addition, he was always accessible and willing to help me with my research.

I would like to thank the rest of my committee members, Professors Kayla Bayless, Carl Gregory and Alvin Yeh for their thoughtful advice and feedback. I also thank my fellow lab mates for the support. They also inspire me in research through our interactions and discussions in the lab.

Last but not the least, my deepest gratitude goes to my family; especially, my parents for their love and support.

TABLE OF CONTENTS

Page

LIST OF FIGURES

Page

LIST OF TABLES

Page

CHAPTER I

INTRODUCTION*

Significant advances have been made in deciphering how mechanical, topographical and biochemical cues within cellular microenvironments that regulate cellular behavior via complex feedback mechanisms involving focal adhesions, cytoskeleton and downstream signaling cascades (Wang, Tytell et al. 2009). In addition to their interactions with soluble cues, cells are also influenced by adhesive interactions with their extracellular matrix (ECM) (Wang, Tytell et al. 2009). ECM is a complex network of molecules that affects multiple processes within each tissue. The mechanical properties and biochemical composition of the ECM varies considerably between tissues. In addition to providing structural support, strength and elasticity, ECM biochemical and mechanical properties influence various cellular behavior and processes like adhesion, differentiation and proliferation, among others.

Actin stress fibers (SFs) are mechanosensitive structural elements of the cytoskeleton that responded to changes in mechanical stimuli to regulate cell morphology, signal transduction, and cell function. SFs within adherent cells generate isometric tension to counterbalance forces in the extracellular matrix and maintain mechanical equilibrium. The exact mechanism by which cell determines their exact response to mechanical

---

*Part of the chapter and the data in this chapter is reprinted from

"Dependence of cyclic stretch-induced stress fiber reorientation on stretch waveform." J Biomech 45(5): 728-735., Tondon, A., H. J. Hsu and R. Kaunas, Copyright (2012), with permission from Elsevier.

stimuli remains unclear. We and others have previously demonstrated that stretch-induced cellular reorganization is dependent on stretch amplitude, frequency and spatial pattern (Jungbauer, Gao et al. 2008, Lee, Haase et al. 2010, Tondon, Hsu et al. 2012). These experiments involved applying different cyclic stretch waveforms in which the strain rates were proportional to the frequency of stretching. Chapter I describes a study in which strain rate and frequency were uncoupled to better understand their respective roles on SF reorganization. We also demonstrated that cells can sense the difference between the strain rates applied during the lengthening and shortening phases of a stretch cycle.

Despite these important insights into the mechanism of cellular response to mechanical stimuli or changes in the mechanical microenvironment, most knowledge in the field has been gained by studying cells cultured on stiff two-dimensional (2-D) substrates. While these systems have provided invaluable insights into cellular responses to tensile strains, there is a growing interest in understanding cell behavior in soft, 3-D tissue-like environments. ECM stiffness is becoming increasingly accepted as an important factor in regulating cell function and actin SFs organization. The extents of cell spreading and SFs formation has been shown to increase with increasing hydrogel stiffness, showing a sharp transition at a stiffness of ~3 kPA (Yeung, Georges et al. 2005). Given that the direction cells align when stretched on silicone rubber depends on actomyosin contractily and contractile activity is low in cells on soft hydrogels, we postulated that stretching cells on a soft substrate would induce cell and SF alignment parallel to the

direction of stretch in a manner dependent on substrate stiffness and actomyosin contractile activity (Chapter II).

Of the 13 million yearly fractures that occur in the United States, about 10% fail to repair (Marsh 1998). Autologous bone grafting procedures are effective, but the available graft material is limited and additional surgery involved has been associated with chronic donor-site pain in many patients. Synthetic bone scaffolds mimic some of the characteristics of bone matrix; however their because of biological incompatibility their effectiveness has been shown to vary. In recent studies, Dr. Carl Gregory's lab had demonstrated that a combination of osteogenically enhanced mesenchymal stem cells (OEhMSCs) and their secreted anabolic extracellular matrix (hMatrix) has an unprecedented ability for the repair of critical-sized defects. The hMatrix is believed to provide an anabolic bone microenvironment and retention signal for the hMSCs at repair site. Polyetheretherketone (PEEK) has increasingly been used in a number of orthopedic implementations, due to its excellent mechanical properties, bioinertness, chemical resistance, and radio-translucency. However, the poor ability of PEEK to support cellular proliferation is unfavorable for many applications where tissue integration is desired. In order to overcome this limitation, we developed a facile technique to modify PEEK surface to allow covalent attachment of hMatrix, with a view to enhance osteointegration (Chapter III).

Malignant bone disease (MBD) can occur by metastasis (e.g. from breast and prostate) or as a result of a primary bone tumor (e.g. osteosarcoma). When tumors establish in bone, catastrophic tissue damage occurs as a result of accelerated bone destruction and

inhibition of repair. The resultant osteolytic lesions (OL) cause pain and fractures and provide an ideal niche for tumor propagation. The OLs accelerate disease progression by providing a supportive stroma for tumor cells. Tumors maintain this microenvironment by secreting factors that prevent mesenchymal stem cells (MSCs) from differentiating into osteoblasts while also stimulating them to secrete tumor survival factors. Our inability to kill resident tumor cells and repair OLs renders MBD terminal in most cases. The key to repairing OLs, and thus treating MBD, lies in understanding the mechanisms by which tumors inhibit osteoblastogenesis. Therefore, in order to study bone-tumor interactions, we developed a novel cell-based disease model of MBD in which human mesenchymal stem cells (hMSCs) and bone tumor cells are co-cultured on osteogenic microsphere in a rotating wall vessel (RWV) to promote the growth of 3D tissue constructs (Chapter IV).

CHAPTER II

EFFECT OF STRETCH WAVEFORM ON STRETCH-INDUCED STRESS FIBER REORIENTATION*

II.A Introduction

Mechanical forces have been known to induce various cellular processes, such as gene expression, protein synthesis, cell migration, proliferation, and differentiation (Banes, Tsuzaki et al. 1995) (Davies and Tripathi 1993, Cappadona, Redmond et al. 1999, Kaspar, Seidl et al. 2002). SFs are mechanosensitive structural elements that responded to changes in cellular mechanical microenvironment to regulate cell morphology, signal transduction, and cell function. SFs consist of bundles of actin – myosin filaments that are anchored to the cell substrate at each end via focal adhesions (Burridge, Fath et al. 1988, Hotulainen and Lappalainen 2006). SFs generate isometric tension to counterbalance forces in the extracellular matrix and maintain mechanical equilibrium (Galbraith and Sheetz 1998). This equilibrium is disrupted by external mechanical cues and SFs can either relax or reorient themselves in an effort to reestablish equilibrium (Hsu, Lee et al. 2009, Kaunas and Deguchi 2011). The dynamics of SF remodeling has only been recently studied through live cell imaging. Hayakawa and colleagues

---

*Part of the chapter and the data in this chapter is reprinted from

"Dependence of cyclic stretch-induced stress fiber reorientation on stretch waveform." J Biomech 45(5): 728-735., Tondon, A., H. J. Hsu and R. Kaunas, Copyright (2012), with permission from Elsevier.

(Hayakawa, Sato et al. 2001) reported that cyclic uniaxial stretch induces SF remodeling through initial disruption of SFs followed by their reassembly at an oblique angle to the direction of stretch.

We and others have demonstrated that stretch-induced SF remodeling is dependent on the frequency of strain application (Kaunas, Nguyen et al. 2005, Hsu, Lee et al. 2010). Furthermore, recent studies investigated the mechanical properties of SFs by observing the retraction of SFs after in situ dissection with a femtosecond laser (Kumar, Maxwell et al. 2006), or a tensile test of isolated SFs (Matsui, Deguchi et al. 2009), and concluded that SFs have viscoelastic properties. In such viscoelastic fibers, the changes in internal tension should be influenced by the waveform of the applied strain. In order to study this here, we perform experiments in which strain rate and frequency are uncoupled to better understand the roles of strain rate and frequency on SF reorganization. We also demonstrate that cells can sense the difference between the strain rates applied during the lengthening and shortening phases of a stretch cycle. These observations were interpreted using a theoretical model of networks of stress fibers with sarcomeric structure. The model predicts that stretch waveforms with fast lengthening rates generate greater average stress fiber tension than that generated by fast shortening. This integrated approach of experiment and theory provides new insight into the mechanisms by which cells respond to matrix stretching to maintain tensional homeostasis. *We have published the finding of this study in the Journal of Biomechanics (Tondon, Hsu et al. 2012).*

II.B Methodology and Results

Stretching setup and strain measurements

Cells were subjected to cyclic stretch using a custom stretch device (Fig. 1) capable of generating various temporal strain waveforms (Table 1). The stretch device consists of two linear motors (Zaber, Canada) that are used to stretch fibronectin-coated silicone rubber chambers (STREX, Japan) seeded with cells as described previously (Lee, Haase et al. 2010) at a density of 1-2X10^5 cells per cm^2. Strains parallel and perpendicular to the principal stretch direction for a nominal stretch of 10% were 0.098 ± 0.009 and -0.020 ± 0.003, respectively, resulting in a Poisson's ratio of 0.19 ± 0.01 (mean ± SD). The entire stretch apparatus was mounted on the stainless steel stage (Gibraltar) of a Nikon FN1 upright microscope housed in a custom-made acrylic enclosure maintained at 37°C using a heat gun (Omega) regulated by a temperature controller (Omega).

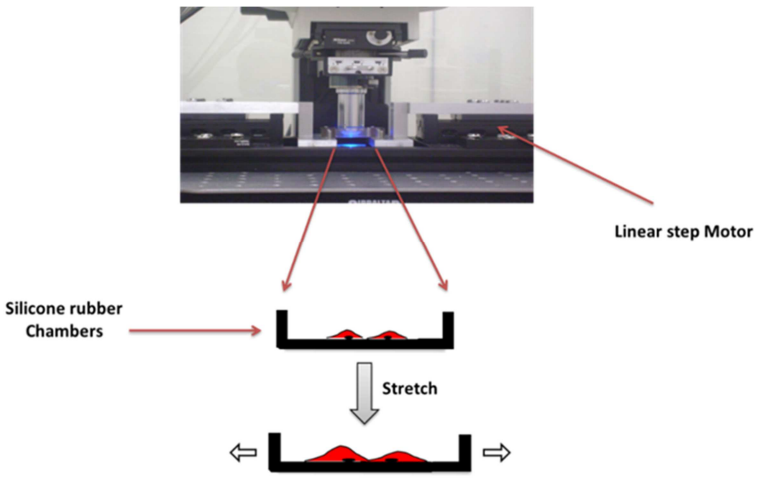

Figure 1. Image of custom built stretch device used to stretch cells.

Table 1. Lengthening and shortening rates for the stretch waveforms. Reprinted from (Tondon, Hsu et al. 2012), with permission from Elsevier.

Waveform	Frequency (Hz)	Lengthening Rate (s^{-1})	Shortening Rate (s^{-1})
Triangle	0.01	0.002	-0.002
	0.1	0.02	-0.02
	1	0.2	-0.2
Square	0.01	2	-2
	0.1	2	-2
Fast-lengthening	0.01	2	-0.001
	0.1	2	-0.01
Fast-shortening	0.01	0.001	-2
	0.1	0.01	-2

Dependence of SFs alignment on the rate of strain rather than frequency

Strain rate in a stretch cycle was proportional to stretch frequency. We hypothesized that the frequency dependence of cyclic stretch-induced SF reorganization may be more precisely defined as a sensitivity to strain rate rather than the frequency of stretching. To test this hypothesis, we subjected the cells to cyclic stretch using a 10% square stretch waveform (hereafter referred to simply as square-stretch) at 0.01Hz (Fig. 2A). The circular variance for each orientation distribution was computed by vectorially summing

the individual orientation vector components, normalizing the result by the total number of vectors (N) and subtracting the obtained number from unity (Mardia and Jupp 2000),

$$Circular\ Variance\ (=1-\frac{1}{N}\sqrt{\left(\sum_{i=1}^{N}\sin 2\theta^{i}\right)^{2}+\left(\sum_{i=1}^{N}\cos 2\theta^{i}\right)^{2}} \quad (1)$$

where θ^{i} is the angle of the ith SF with θ^{i} defined as 0° along direction of stretch. The angles were doubled to accurately account for the bi-directionality of axial vectors, i.e. $2\theta = 2(\theta + 180°)$. The values range from 0 to 1, corresponding to perfectly aligned and totally uniform distributions, respectively. The frequency of stretch was the same as for 0.01Hz triangle-stretch, but the rates of lengthening and shortening were much higher. Square-stretch at 0.01Hz induced significant cell alignment perpendicular to the direction of stretch (Fig. 2B). Further, 0.01Hz square-stretch induced significant SF alignment with a smaller circular variance than that achieved with 0.1Hz triangle-stretch (0.69 vs. 0.79). Increasing the frequency of square-stretch to 0.1Hz further decreased the circular variance to 0.49 (Figs. 2C).

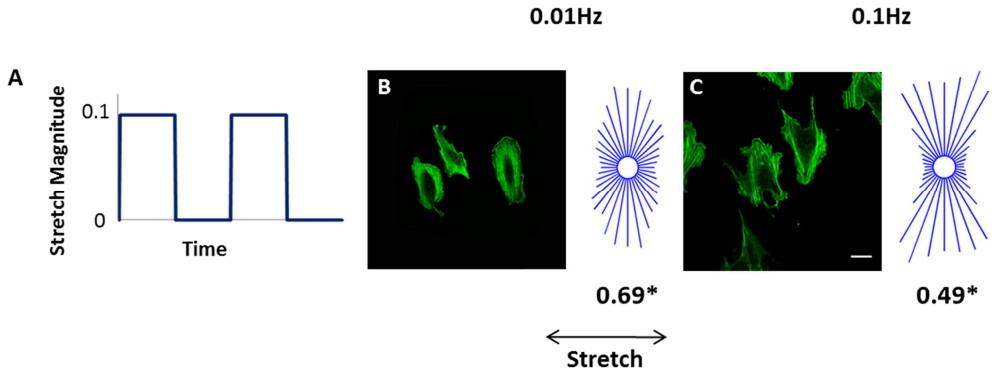

Figure 2. Square-stretch at low frequency induces SF alignment. Two cycles of 10% cyclic square-stretch are shown (A). Representative images and circular histograms depicting SF angular distributions of non-confluent U2OS cells (n = 90 for each condition) subjected to 12h square-stretch at 0.01 (B) and 0.1Hz (C). Bar, 25 μm. Reprinted from (Tondon, Hsu et al. 2012), with permission from Elsevier.

Live cell microscopy was performed to observe the dynamics of SF reorganization in response to 0.01Hz square-stretch (Fig. B.1). Initially, the cell contained SFs that were oriented roughly parallel to the axis of stretching. Although the SFs did eventually become aligned perpendicular to the direction of stretch, the entire process took ~10h. Similar slow alignment was observed when repeating this experiment for four cells, indicating that these results are representative for the U2OS cell response to 10% cyclic uniaxial stretch at 0.01Hz. Thus, the dynamics of SF reorientation in response to 0.01Hz square-stretch were considerably slower for than for 1Hz triangle-stretch.

Fiber lengthening rate has a greater effect on the resulting SFs alignment than fiber shortening rate

Cyclic stretch involves lengthening and shortening phases, and the rates of these phases were of equal magnitude for triangle- and square-stretch. To assess the effects of the rate of lengthening and shortening independently, asymmetric strain waveforms were applied using the same fast strain rate as used for square-stretch, but with a slow rate of strain in the opposite phase of the cycle (Figs. 3A and D). Hereafter, these asymmetric waveforms will be referred to as fast-lengthening-stretch and fast-shortening-stretch. The SFs in cells subjected to fast-lengthening-stretch for 12h at 0.01Hz aligned to a comparable extent as SFs in cells subjected to 0.01Hz square-stretch (Figs. 3B vs. 2B). Similarly, fast-lengthening-stretch at 0.1Hz resulted in comparable SF alignment to that caused by 0.1Hz square-stretch (Figs. 3C vs. 2C). Fast-shortening-stretch resulted in no SF alignment at 0.01 (Fig. 3E) and very little alignment at 0.1Hz (Fig. 3F). At 1Hz, both asymmetric waveforms resulted in SF alignment to an extent similar to that for triangle-stretch at 1Hz.

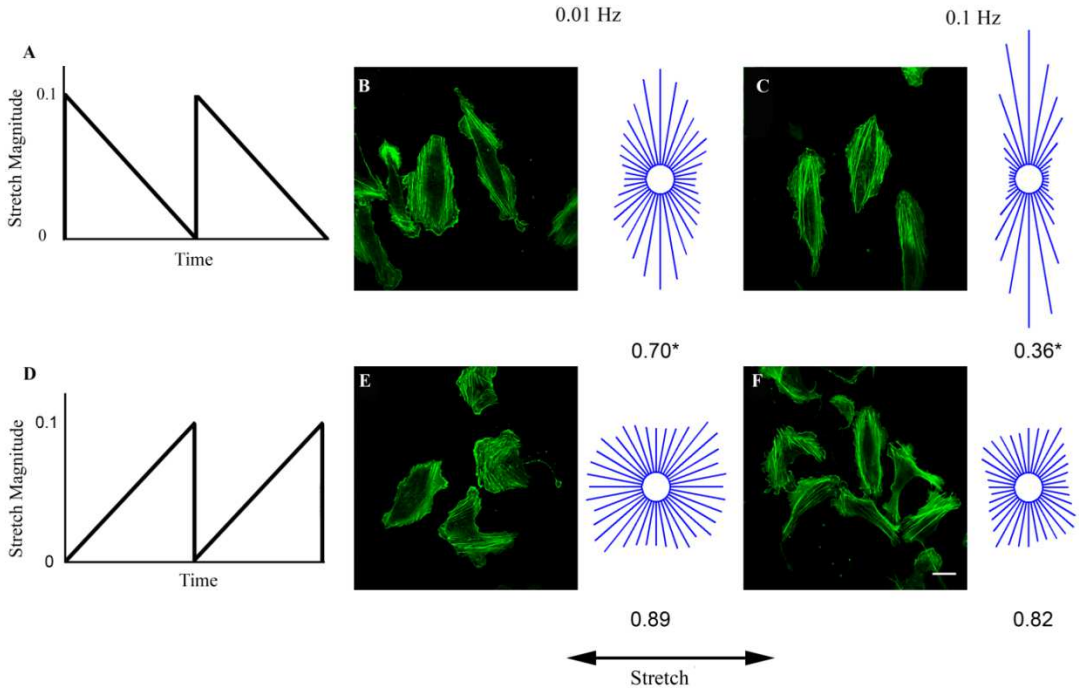

Figure 3. SFs align in response to lengthening, rather than shortening, rate. A, D: Two cycles of 10% cyclic fast-lengthening-stretch (A) and fast-shortening-stretch (D). Representative images and circular histograms of non-confluent U2OS cells (n = 90 for each condition) subjected to 12 hr of fast-lengthening-stretch at 0.01 (B) and 0.1Hz (C) and fast-shortening-stretch at 0.01 (E) and 0.1Hz (F). Bar, 25 μm. Reprinted from (Tondon, Hsu et al. 2012), with permission from Elsevier.

Statistical comparisons between conditions were performed by computing the average value for cos2θ for each cell imaged and then averaging these values for all cells at each condition (⟨cos2θ⟩). Uniform or randomly distributed stress fibers would result in ⟨cos2θ⟩ = 0, alignment perpendicular to stretch would result in a value of -1, and alignment parallel to stretch would result in a value of +1. At 0.01Hz (Fig. 4A) and

0.1Hz (Fig. 4B), stretching waveforms with fast lengthening rates (i.e. square-stretch and fast-lengthening-stretch) resulted in significantly lower values for ⟨cos2θ⟩ than those for stretch waveforms with slow lengthening rates (i.e. triangle-stretch and fast-shortening-stretch).

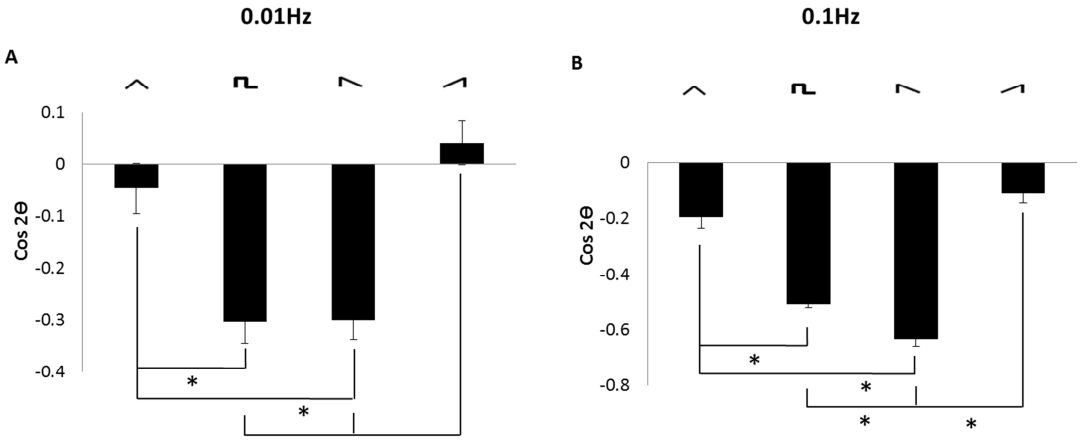

Figure 4. Stretch patterns with fast lengthening result in greatest alignment. Distributions in the values of cos 2θ values for each individual cells at each condition (mean ± SEM) at 0.01(A) and 0.1Hz (B) are shown to quantify the extent of alignment. * indicates significant differences between groups as determined by ANOVA followed by Student-Neuman-Keuls post-hoc multiple comparison testing ($P < 0.01$). Reprinted from (Tondon, Hsu et al. 2012), with permission from Elsevier.

Interpretation of the results using theoretical modeling

Figure 5 shows comparisons in the angular histograms measured from the experiments and those generated from solving the model under identical stretching waveforms at 0.01

and 0.1Hz. The level of tension in SFs within intact cells undergoing cyclic stretching has not been measured. Time-dependent changes in SF tension can be predicted using theoretical models, however (Hsu, Lee et al. 2010). The population-average SF tension $\langle f \rangle$ varies over the first several cycles of stretch until achieving a dynamic steady-state response for each condition (Fig. 6). At 0.01Hz, triangle-stretch generates an imperceptible perturbation in tension (amplitude of $0.02f_0$) since the strain rate is very small (Fig. 6A). The amplitude in tension perturbation does become apparent ($0.15f_0$) at 0.1Hz. At both 0.01 and 0.1Hz, the rapid lengthening rates in square-stretch generate a rapid rise in tension that decays back to f_0 within 5s during the first half of the stretch cycle, followed by a rapid drop in tension the decays back to f_0 within 5s during the latter half of the cycle. The response to fast-lengthening-stretch at 0.01 and 0.1Hz (Fig. 6B) closely resembles the response to the first half of the cycle for square-stretch, with a rapid rise in tension occurring at the beginning of each cycle. The response to fast-shortening-stretch at 0.01 and 0.1Hz mirrors the response to fast-lengthening-stretch, with a rapid fall in tension occurring at the end of each cycle. At 0.1Hz, the asymmetric waveforms do not result in tension returning to $f_0$during the periods of slow strain since the strain rate is sufficiently high to cause a small perturbation in tension. At 1Hz, the responses take 5s to reach steady-state and all the waveforms generate comparably large positive perturbations in tension ($>f_0$) since the SFs do not have enough time between cycles to relax (Fig. 6A and B). Since these perturbations are of comparable size, each of the waveforms tested are predicted to result in a similar extent of stress fiber alignment at 1Hz. In summary, the model is able to predict SF orientation distributions similar to

that observed in our experiments (cf. Fig. 6) and also predicts that the SFs are induced to reorganize in response to positive perturbations in SF tension.

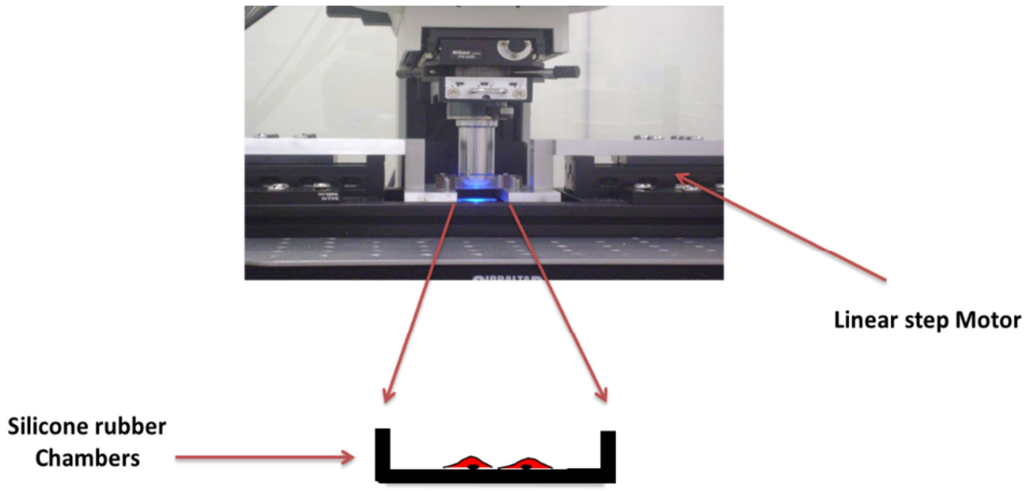

Figure 5. Image of custom built stretch device used for subjecting cells to different temporal stretch patterns.

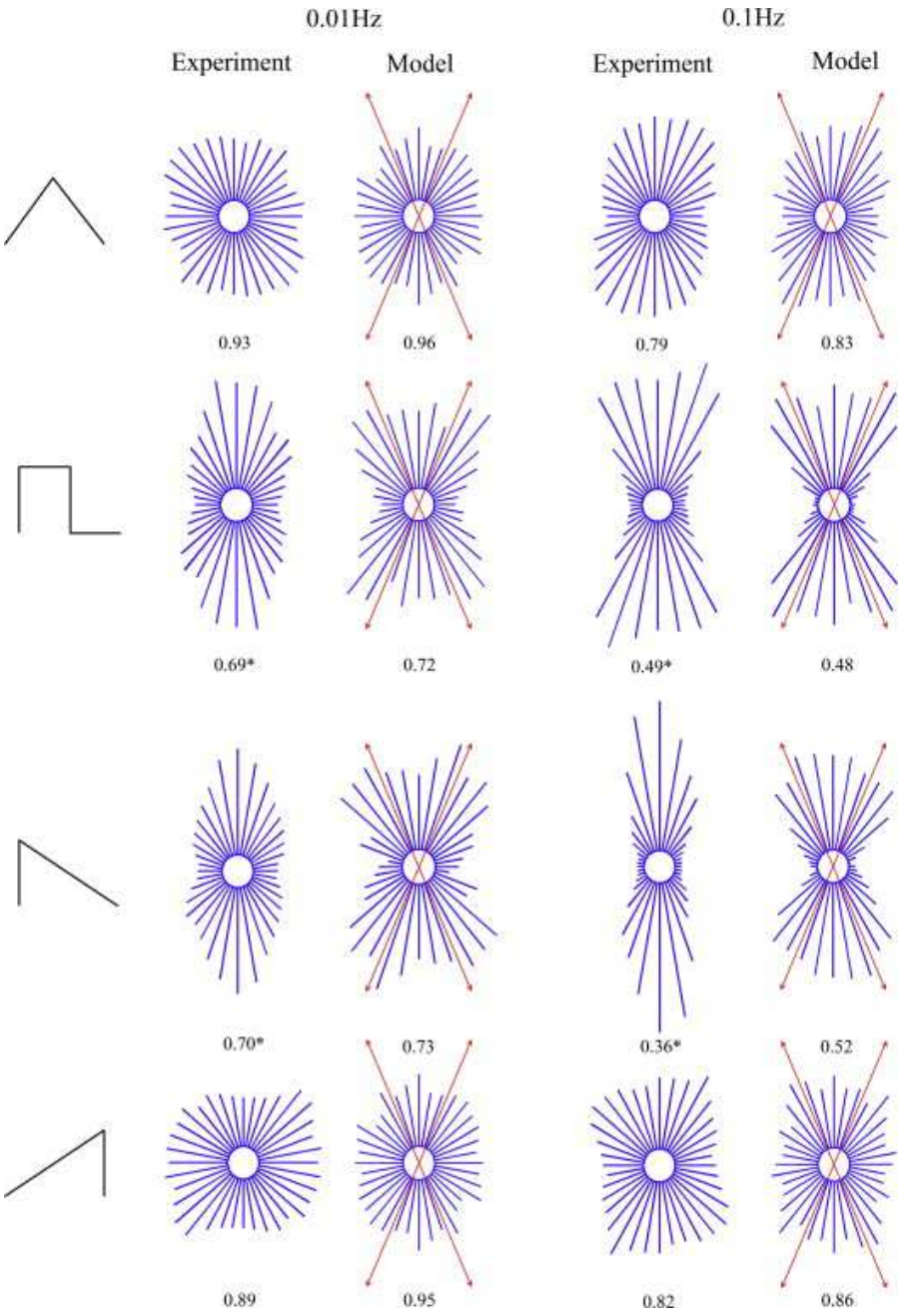

Figure 6. Comparisons of measured and simulated SF alignment distributions. Circular histograms depicting the experimentally measured and theoretically predicted SF distribution in cells subjected to 12 hours of stretching using the various strain patterns. Red arrows indicate the preferred orientations (±67□ relative to the direction of stretch) of SFs as predicted by the model. Reprinted from (Tondon, Hsu et al. 2012), with permission from Elsevier.

II.C Discussion

We and others have reported that uniaxial cyclic stretch induces cell and SF alignment, with the extent of alignment dependent on stretch amplitude, frequency and spatial pattern (Wang, Goldschmidt-Clermont et al. 2001, Kaunas, Nguyen et al. 2005, Kaunas, Usami et al. 2006, Jungbauer, Gao et al. 2008). This is the first study to carefully examine the effects of the shape of the temporal waveform on stretch-induced SF reorganization. The results clearly demonstrate that cells are more responsive to strain rate than stretch frequency *per se*.

Previous studies have reported that rapid shortening of SFs causes their disassembly (Costa, Hucker et al. 2002, Sato, Adachi et al. 2005), suggesting that the rate of shortening would be important in cyclic stretch-induced SF reorganization. Several lines of evidence in the current study support the conclusion that the rate of lengthening has a much stronger effect than the rate of shortening on SF alignment. First, the extent of alignment was similar for both square-stretch and fast-lengthening-stretch at 0.01Hz (cf. Fig. 6A) and 0.1Hz (cf. Fig. 6B). Second, there was no alignment in response to triangle-stretch and fast-shortening-stretch at 0.01Hz (cf. Figs. 1A , 4E and 6A). Finally, the circular variance was slightly smaller for fast-shortening-stretch at 0.1Hz than at 0.01Hz (Figs. 4C vs. 4B), which could be attributed to the relatively fast lengthening rate ($0.01s^{-1}$ vs. $0.001s^{-1}$). Shortening induced SF disassembly observed in previous reports required the application of relatively large magnitudes of shortening (>20%) that were sufficient to cause SF buckling and complete loss of tension (Costa, Hucker et al. 2002,

Sato, Adachi et al. 2005). We applied stretch with an amplitude of 10%, which may be too low for shortening to have a significant effect since the SFs are predicted to be under tension at all times. We have previously demonstrated that SFs in U2OS cells expressing GFP-actin do not suddenly disassemble in response to 10% step increase or decrease in equibiaxial stretch (Hsu, Lee et al. 2010). In the case of a 0.01Hz square-wave waveform with rapid lengthening and shortening applied repeatedly, SFs required several hours to gradually become reoriented perpendicular to the direction of stretch.

The level of tension in SFs within intact cells undergoing cyclic stretching has not been measured. Time-dependent changes in SF tension can be predicted using theoretical models, however. A model developed by our lab predicts that myosin II within sarcomeres responds to perturbations in tension at a rate dependent on myosin cross-bridge cycling (cf. Eqn. 1). Specifically, the model predicts that at low strain rates, myosin sliding can relax perturbations in tension even though the SF is cyclically lengthening and shortening. At high strain rates, the model predicts that myosin cannot respond quickly enough to relax these perturbations.

There are only a few models of stretch-induced SF reorganization that are capable of describing the effects of strain rate. The model by Wei et al. (2008) predicts that actin is more likely to depolymerize in directions of rapid shortening, resulting in frequency-dependent SF alignment perpendicular to the direction of stretch. Their model is not consistent with our observation that SFs are not induced to align in response to rapid shortening. De et al. (2007) proposed a coarse-grained model which also predicts

frequency-dependent alignment, but it is not clear that their model is capable of predicting of the effects of asymmetric waveforms.

The ability of our model to describe the differential effects of asymmetric waveforms with rapid lengthening vs. rapid shortening relies on the asymmetric dependence of positive vs. negative perturbations in tension from stall force f_0 (cf. Fig. 5). According to Eqn. 2, this asymmetry is due to the contribution of load-induced bond breaking, though we do not have sufficient information to identify which specific bonds are affected. Likely candidates include actomyosin interactions, integrin-matrix bonds and interactions between focal adhesion proteins.

GFP-actin has been reported to be a suitable, intrinsic probe of both the organization and dynamics of the actin cytoskeleton in Swiss 3T3 and NIH 3T3 fibroblasts (Choidas, Jungbluth et al. 1998). However, stress fibers in rat embryonic fibroblasts transiently transfected with pEYFP-β-actin were recently reported to be unable to align perpendicular to cyclic stretch and to exhibit an atypical morphology (Deibler, Spatz et al. 2011). The U2OS cells stably-expressing GFP-β-actin used in the present study behaves similarly to bovine aortic endothelial cells when subjected to cyclic uniaxial stretch by both aligning perpendicular to stretch direction and reaching a steady state after approximately 2hr of stretching (Hsu, Lee et al. 2009, Lee, Haase et al. 2010).

It is surprising that SF alignment appeared clearly unimodal in most cases where significant SF alignment occurred (cf. Figs. 1D, 2B, 4B and 4C). Our model, and that of Takemasa et al. (1998), predict that SFs would preferentially align at an angle of ±67°

relative to the direction of stretch since this is the direction of least perturbation in SF length. Only in the case of 0.1Hz square-stretch (cf. Fig. 2C) did the distribution appear to follow these model predictions. It is unclear at this point what the causes for the discrepancies in preferred orientation are at this point, however.

II.D Conclusion

Cyclic uniaxial stretching of adherent nonmuscle cells induces the gradual reorientation of their actin stress fibers perpendicular to the stretch direction to an extent dependent on stretch frequency. By subjecting cells to various temporal waveforms of cyclic stretch, we revealed that stress fibers are much more sensitive to strain rate than strain frequency. By applying asymmetric waveforms, stress fibers were clearly much more responsive to the rate of lengthening than the rate of shortening during the stretch cycle. These observations were interpreted using a theoretical model of networks of stress fibers with sarcomeric structure. The model predicts that stretch waveforms with fast lengthening rates generate greater average stress fiber tension than that generated by fast shortening. This integrated approach of experiment and theory provides new insight into the mechanisms by which cells respond to matrix stretching to maintain tensional homeostasis.

CHAPTER III

INTERACTIVE EFFECTS OF MATRIX STRAIN AND STIFFNESS ON CELL AND STRESS FIBER REORGANIZATION

III.A Introduction

In the past decades, ECM stiffness has been shown to strongly regulate many cell processes, including cell–cell adhesion (Wang, Tolic-Norrelykke et al. 2002, Reinhart-King 2008), cell–substrate adhesion (Reinhart-King, Dembo et al. 2008), and cell differentiation (Engler, Bacakova et al. 2004). For example, stem cells cultured on substrates with stiffness approaching that of a particular tissue tend to appear like, and differentiate into, cells typically resident of that tissue (Engler, Sen et al. 2006).Theoretical modeling indicates that it is the stiffness of the cell relative to that of the substrate that governs stem cell internal structure and morphology (Zemel, Rehfeldt et al. 2010).

A key event in adaptive cellular structural remodeling and rigidity-sensing is the modulation of cellular contractility (Fouchard, Mitrossilis et al. 2011). Cells have been shown to generate greater traction forces, have more stable focal adhesion sites, generate more stable and defined actin SFs and spread more extensively on rigid surfaces than on soft compliant surfaces. Since the organization of SFs in cells subjected to stretch depends on the levels of both externally applied and internally generated forces, it follows that matrix rigidity would influence cellular responses to stretching.

In this study, we investigated the roles of matrix properties and stretching patterns on cell structure by uniaxially stretching U2OS cells expressing GFP-actin on silicone rubber sheets supporting either a surface-adsorbed coating or thick hydrogel of type-I collagen. Cells and their actin stress fibers oriented perpendicular to the direction of cyclic stretch on collagen-coated sheets, but oriented parallel to the stretch direction on collagen gels. There was significant alignment parallel to the direction of a steady increase in stretch for cells on collagen gels, while cells on collagen-coated sheets did not align in any direction. The extent of alignment was dependent on both strain rate and duration. Stretch-induced alignment on collagen gels was blocked by the myosin light-chain kinase inhibitor ML7, but not by the Rho-kinase inhibitor Y27632. We propose that active orientation of the actin cytoskeleton perpendicular and parallel to direction of stretch on stiff and soft substrates, respectively, are responses that tend to maintain intracellular tension at an optimal level. Further, our results indicate that cells can align along directions of matrix stress without collagen fibril alignment, indicating that matrix stress can directly regulate cell morphology. *We published the finding of this study in* PLOS ONE *(Tondon and Kaunas 2014).*

III.B Methodology and Results

Stretching setup and strain measurements

Silicone rubber stretch chambers (STREX, Japan) were modified to form a circular well (15 mm diameter) by adhering a silicone rubber sheet onto the chambers (Fig. 5 & 7). The chambers were initially coated with collagen (4 μg/cm^2) by incubating 100 μl of 0.3

mg/ml rat tail collagen type I (BD Biosciences) in the well and allowing the solution to evaporate. The collagen solution (3 mg/ml) was then added to form a gel within the collagen-coated well as described previously (Kang, Kwak et al. 2011). Cells were cultured on the top surface of the collagen gels and subjected to cyclic stretch using our custom built stretch system described above.

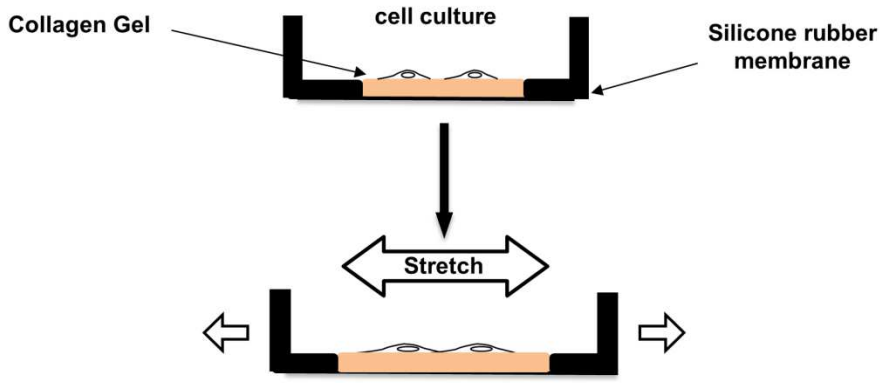

Figure 7. Silicone rubber chamber with collagen gel before and after stretch.

The strain fields produced by the device were determined by tracking the displacement of markers on the collagen gel and silicone rubber surfaces. Strains on the bottom surface of the silicone rubber sheeting were measured by marking membranes at several points with a permanent marker and imaging before and after stretch using nominal stretch values ranging from 2.5 to 12.5%. To quantify the strains on the collagen gel surface, red fluorescent beads (0.2 µm Fluospheres, Molecular Probes) were mixed into

the gel prior to polymerization to serve as fiducial markers. Triads of markers in a focus plane in various locations on the surface were selected to compute the symmetric Lagrangian strain tensor at each location. The finite strains in the longitudinal (E1) and lateral directions (E2) were computed from the E11 and E22 components of the Lagrangian strain tensor (Fung 1994) using Eqns. 2A and 2B.

$$E_1 = \sqrt{1+2E_{11}} - 1 \tag{2A}$$

$$E_2 = \sqrt{1+2E_{22}} - 1 \tag{2B}$$

Two-dimensional strains measured on the surfaces of 500 µm-thick collagen gels and the supporting silicone rubber membranes were very similar (Fig. 8). Strains parallel and perpendicular to the principal stretch direction on surface of collagen for a nominal stretch of 10% were 0.093±0.009 and −0.040±0.01 (Fig. 8A and 8B), respectively, resulting in a Poisson's ratio of 0.43±0.01 (mean±SD). Strains observed on the surface of silicone rubber membranes were 0.097±0.01 and −0.046±0.005 parallel and perpendicular to that of principal stretch direction, respectively, resulting in a Poisson's ratio of 0.47±0.05 (mean±SD).

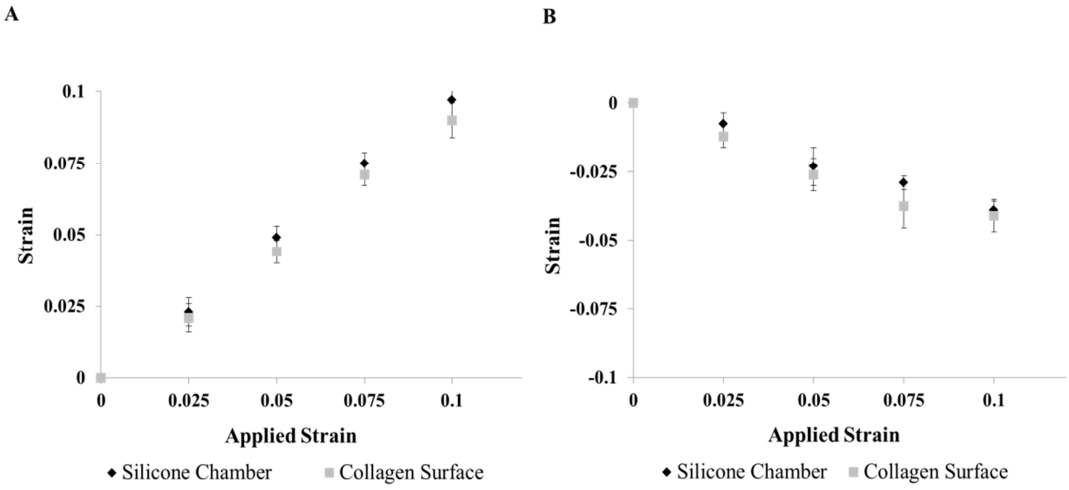

Figure 8. Strain is efficiently transmitted to the collagen gel surface. The longitudinal (A) and lateral (B) strains (mean ± SEM; n=6) within the region of the silicone rubber chamber used to support the collagen gels were quantified at the surfaces of the silicone rubber sheet (black) and the collagen gel (grey). Reprinted from (Tondon and Kaunas 2014)

Cyclic stretch-induced SF alignment depend on the thickness of the collagen gel

Given that the direction cells align when stretched on silicone rubber depends on actomyosin contractile activity and contractile activity is low in cells on soft hydrogels, we postulated that stretching cells on a soft substrate would induce cell and SF alignment parallel to the direction of stretch in a manner dependent on substrate stiffness and actomyosin contractile activity. In order to test this, we evaluated the effects of stretch on SF organization in non-confluent U2OS cells adhered onto the top of a 500 μm thick collagen gels. For comparison, experiments were also performed where the

cells were adhered on the supporting silicone rubber membranes, but coated with a low concentration of collagen (4 $\mu g/cm^2$) rather than the thick gel. In each case, the cells were subjected to 3h of 10% cyclic uniaxial stretch at 1Hz. Consistent with our previous findings using non-confluent and confluent U2OS and bovine aortic endothelial cells on fibronectin-coated silicone rubber (Hsu, Lee et al. 2009, Lee, Haase et al. 2010, Tondon, Hsu et al. 2012), the SFs in cells on collagen-coated silicone rubber oriented perpendicular to the direction of stretch (Fig. 9A). In contrast, the cells and their SFs reoriented parallel to the direction of stretch on thick collagen gels (Fig. 9B). To determine if the result was cell type –specific, the experiments were repeated using human mesenchymal stem cells (Figs. 9C and D). Confocal reflectance images of collagen fibers in regions containing a cell (Fig. 9E) and regions devoid of cells (Fig. 9F) indicated that collagen fibrils did not co-align with the cells in response to cyclic stretching.

To determine the dependence on strain rate on thick collagen gels, the extent of cell and SF alignment was quantified in U2OS cells subjected to 3h of 10% cyclic uniaxial stretch at 0.01, 0.1 and 1Hz on collagen gels. At 0.01Hz, there was no cell or SFs alignment in any direction (Figs. 10A, D and E). Increasing the frequency of stretch to 1Hz significantly increased alignment parallel to the stretch direction (Figs. 10C, D and E), while stretching at 0.1Hz had an intermediate response (Figs. 10B, D and E). These results were consistent with the frequency-dependence we previously observed when stretching endothelial and U2OS cells on fibronectin-coated silicone rubber sheets (Hsu, Lee et al. 2010, Lee, Haase et al. 2010)

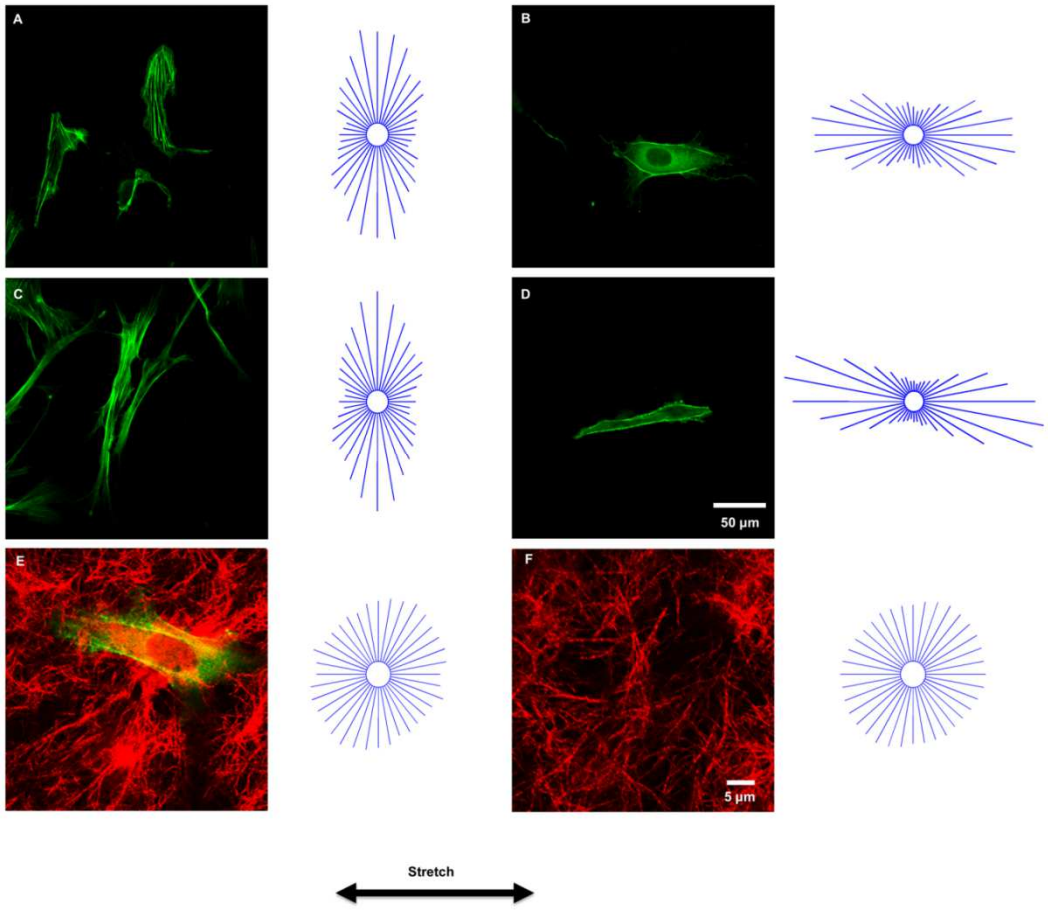

Figure 9. Cyclic stretch-induced SF alignment on soft collagen gels and stiff silicone rubber sheets. A-D: Representative images and circular histograms depicting SF angular distributions of non-confluent U2OS cells (A, B) (n = 90 for each condition) and hMSCs (C, D) (n = 60 for each condition) subjected to 3h of 10% cyclic uniaxial stretch at frequency of 1Hz on collagen-coated rubber sheets (A, C) and collagen gels (B, D). Scale bar, 50 µm. E, F: Representative confocal reflectance images of collagen fibrils (red) in regions containing a U2OS cell (E) and devoid of cells (F) and circular histograms depicting collagen fibril alignment after 3h of 10% cyclic stretching at 1Hz.; Scale bar, 5 µm. Reprinted from (Tondon and Kaunas 2014)

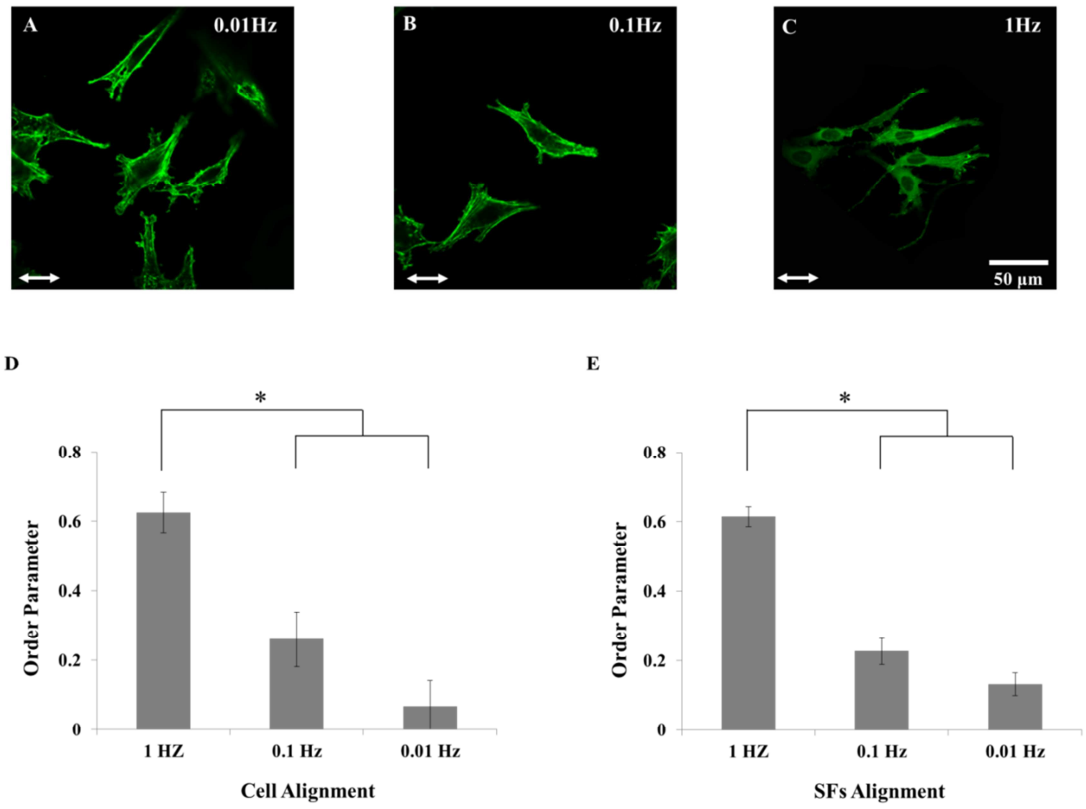

Figure 10. Cyclic stretch-induced cell and SF alignment on soft collagen gels depends on stretch frequency. Representative images of non-confluent U2OS cells adhered on a soft collagen matrix subjected to 3h of 10% cyclic stretch at frequencies of 0.01 (A), 0.1 (B) and 1Hz (C). Order parameters for cells (D) and SFs (E) were computed for each cell to quantify the extents of alignment and the results were summarized (mean ± SEM; n = 90). * indicates significant differences between groups as determined by ANOVA followed by Student-Neuman–Keuls post-hoc multiple comparison testing ($P<0.01$). Scale bar, 50 µm. Reprinted from (Tondon and Kaunas 2014)

Cells and their SFs align in response to step stretch on cells adhered onto thick collagen gels, but not on collagen-coated silicone rubber sheets

Gavara et al. (2008) reported that collagen type I hydrogels (1.45 mg/ml) have a stiffness of 23 Pa that increased to 137 Pa in response to a step equibiaxial stretch of 11% (Gavara, Roca-Cusachs et al. 2008). Previous studies indicate that uniaxial stretching a collagen gel causes anisotropic changes in gel stiffness, with the stiffness increasing in the direction of stretching (Girton, Barocas et al. 2002, Vader, Kabla et al. 2009). To determine if anisotropic changes in gel stiffness contribute to cell and SF alignment, U2OS cells were cultured on collagen gels that were subjected to 10% uniaxial pre-stretch prior to cell attachment (Fig. 11A). After 6h, there was significant cell (Fig. 11E) and SF (Fig. 11F) alignment parallel to the direction of matrix stretching. In contrast, there was no alignment observed in cells cultured on pre-stretched collagen-coated silicone rubber.

Next, we quantified the effects of applying the stretch after the cells had spread. A rapid stretch of 20%/s (Fig. 11B) resulted in an apparent increase in cell alignment (Fig. 11E) and a significant increase in SF alignment (Fig. 11F) relative to that induced by seeding cells on a pre-stretched gel. A slow stretch at 0.2%/s (Fig. 11C) induced significantly less cell and SF alignment than both the pre-stretch and rapid stretch treatments (Figs. 11E-F). Interestingly, a rapid stretch applied to cells on collagen-coated silicone rubber (Fig. 11D) did not induce any alignment (Figs. 11E-F).

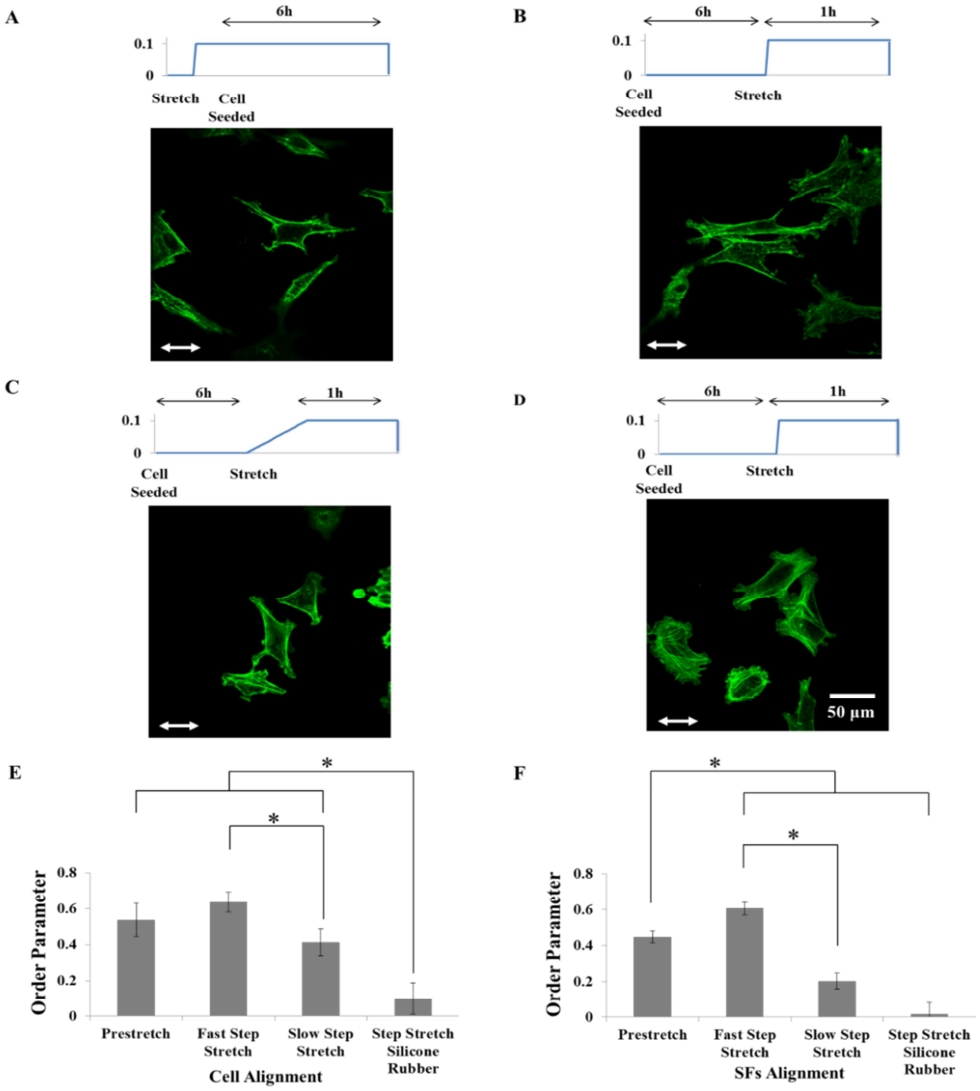

Figure 11. Effects of pre-stretch and strain rate on steady stretch-induced cell and SF alignment. Representative images of non-confluent U2OS cells seeded on 10% pre-stretched collagen gel (A) or adhered onto collagen gels (that were not pre-stretched) subjected to 10% stretch at ramp rates of 20%/s (B) and 0.2%/s (C). Representative image of U2OS cells adhered onto collagen-coated silicone rubber sheets subjected to 10% stretch at 20%/s (D). Cell (E) and SF (F) order parameters (n = 90) are summarized. * indicates significant differences between groups as determined by ANOVA followed by Student-Neuman–Keuls post-hoc multiple comparison testing ($P<0.01$).Scale bar, 50 µm. Reprinted from (Tondon and Kaunas 2014)

Extent of cell and SF alignment depends on the duration of transient step stretch

To assess the effects of the duration of stretching, we subjected the cells adhered on collagen gels to 10% transient step stretch, i.e. a regimen consisting of a rapid ramp increase in stretch (20%/s), a transient hold (10s, 10min or 1h), and subsequent release of the stretch (Figs. 12A-C). In each case, the cells were fixed after a total elapsed time of 1h. No alignment of cell or SFs occurred in response to 10s of transient stretch (Figs. 12D and E). There was significantly more cell and SFs alignment in response to 1h of transient stretch, while 10min of transient stretch resulted in an intermediate response.

Role of MLCK in SF formation and reorientation

Consistent with previous findings with NIH 3T3 fibroblasts on soft polyacrylamide gels (Yeung, Georges et al. 2005), we observed that SFs were less prevalent in cells on soft collagen hydrogels as compared to cells on stiff collagen-coated silicone rubber sheets (cf. Figs. 9B vs. 9A). Further, the few SFs observed in cells adhered onto soft collagen gels were primarily located in the cell periphery (cf. Figs. 9B and 9D). In contrast, both peripheral and central SFs were observed in cells on collagen-coated silicone rubber (cf. Figs. 9A and 9C). We have previously shown that Rho-kinase and myosin light-chain kinase (MLCK) regulate different populations of SFs: peripheral SFs are sensitive to MLCK inhibition, while central SFs are sensitive to Rho-kinase inhibition (Lee, Haase et al. 2010).

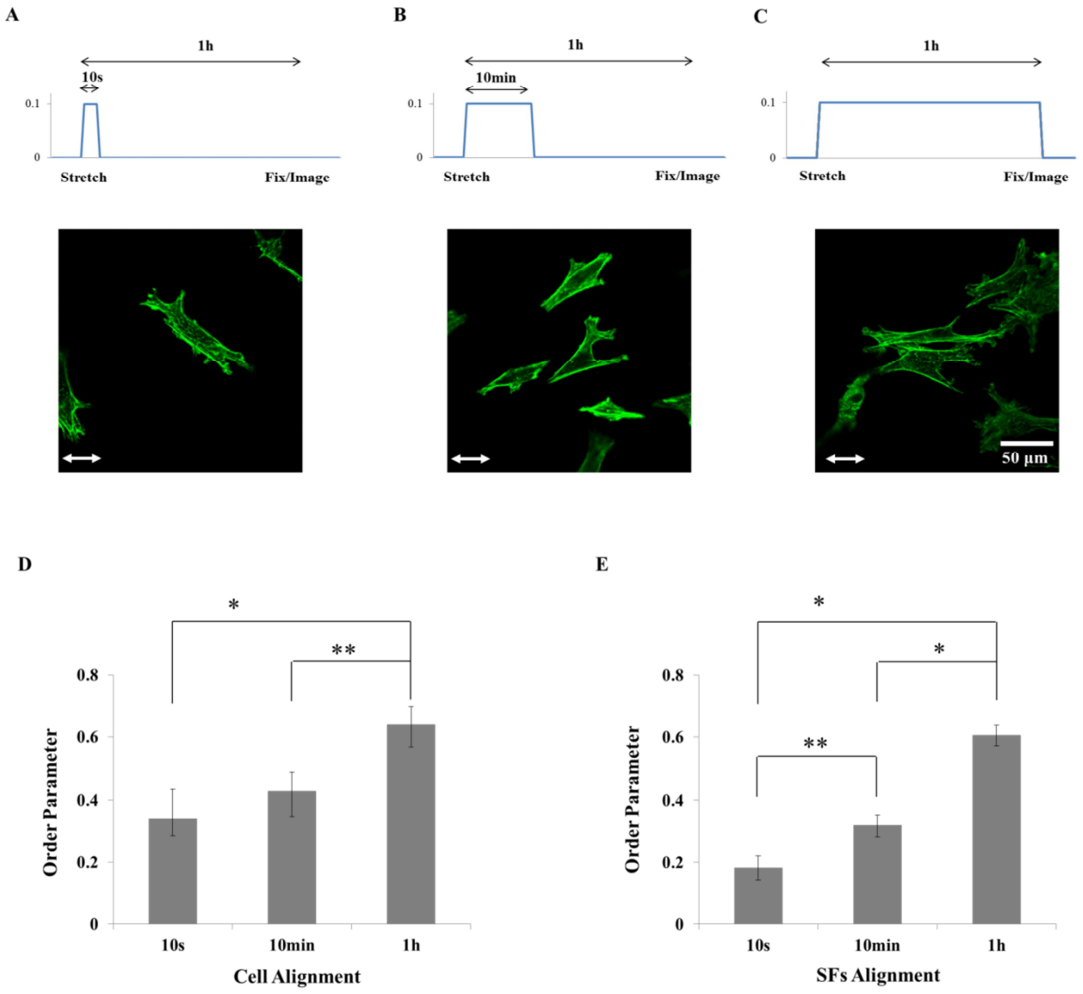

Figure 12. Extent of cell and SF alignment depends on the duration of transient step stretch. Representative images of non-confluent U2OS cells adhered onto collagen gels subjected to 10% transient step stretch, i.e. a regimen consisting of rapid ramp increase in stretch, a hold, and subsequent release of the stretch. The collagen gels were subjected to 10% stretch and held for 1s (A), 10min (B) and 1h (C). Cell (E) and SF (F) order parameters (n = 90) are summarized. Significant differences between groups were determined by ANOVA followed by Student-Neuman–Keuls post-hoc multiple comparison testing (* = P<0.01, ** = P<0.05). Scale bar (A-C), 50 µm. Reprinted from (Tondon and Kaunas 2014)

To assess the involvement of MLCK and Rho-kinase pathways in stretch induced SF alignment on cells adhered to collagen gels, we treated the U2OS cells with inhibitors of either MLCK (ML7) or Rho-kinase (Y27632) and subjected them to 10% cyclic stretch at 1Hz for 3h (Fig. 13). The cells were treated with either 10 µM Y27632 or 30 µM ML7 for 30 min prior to initiating stretch with the drug remaining in the culture media throughout the experiment. In cells treated with ML7, SFs were completely attenuated (Fig. 13A). In contrast, there was some reduction in the number of SFs in cells treated with Y27632, but these remaining fibers oriented roughly parallel to the direction of cyclic stretch (Fig. 13B).

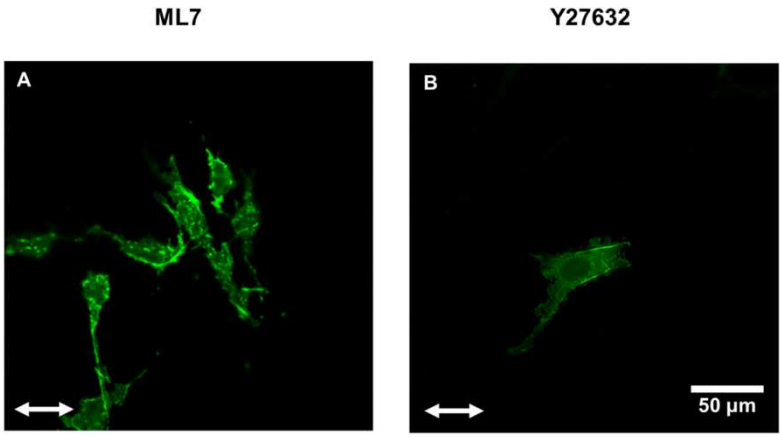

Figure 13. Roles of Rho-kinase and MLCK on cyclic stretch-induced SF alignment in cells on 3-D collagen gels. Representative images of non-confluent U2OS cells (n = 60) adhered on soft collagen gels subjected to 3h of 10% cyclic uniaxial stretch at 1Hz after treatment with 30µM ML7 (A) or 10µM Y27632 (B). Scale bar, 50 µm. Reprinted from (Tondon and Kaunas 2014)

III.C Discussion

Our results demonstrate that stretch-induced cell and SF alignment are highly dependent on the mechanical properties of the collagen matrix upon which cells are cultured. Cyclic stretch promoted alignment parallel to the direction of stretch (cf. Figs. 9B and 9D) in cells with attenuated contractility caused by adhesion to a soft collagen gel, as judged by the relatively few SFs relative to that in the same cell type on collagen-coated silicone rubber. This is consistent with previous studies performed with cells on fibronectin-coated silicone rubber showing that stretching promotes SF alignment parallel to the direction of stretch when cell contractility is attenuated with small molecule inhibitors of Rho-kinase or MLCK (Kaunas, Nguyen et al. 2005, Lee, Haase et al. 2010). This is in stark contrast to the perpendicular alignment observed when cell contractility is at normal levels for cells on silicone rubber coated with collagen (cf. Figs. 9A and 9C) or fibronectin (Kaunas, Nguyen et al. 2005). In the case of a step stretch, cell and SF alignment was only observed on soft collagen gels, but not on silicone rubber coated with collagen (cf. Figs. 11E-F)) or fibronectin (data not shown).

We previously reported a theoretical model predicting that SFs reorient perpendicular to the direction of cyclic stretch on matrix-coated silicone rubber to avoid excessive levels of tension acting on actomyosin binding sites (Hsu, Lee et al. 2009, Hsu, Lee et al. 2010, Kaunas and Deguchi 2011, Tondon, Hsu et al. 2012). On relatively stiff silicone rubber sheets, where SF tension is already high under static conditions, the model predicts that tension is at an optimal level. Cyclic stretching at a high strain rate perturbs tension from

this optimal level, promoting the disassembly of SFs and their preferred reassembly in an orientation perpendicular to the direction of stretch to minimize perturbations in tension. Since SF tension in cells on soft collagen gels is relatively low, we speculate that stretching increases tension toward the optimal level found in cells on a stiffer substrate, thereby promoting SF alignment parallel to the direction of stretch. The data herein provides the motivation for future development of our model to explicitly describe the role of substrate stiffness.

U2OS cell line was originally cultivated from moderately differentiated sarcoma of the tibia of a fifteen-year-old human female suffering from osteosarcoma. U2OS cells exhibit epithelial adherent morphology (Ponten and Saksela 1967). We observed that U2OS cell spreading and cytoskeleton architecture was similar to that of bovine aortic endothelial cells when cultured on both coated silicone rubber and soft collagen gels. Actin SFs in U2OS cells expressing GFP-actin respond to cyclic stretching by reorienting perpendicular to the direction of stretch with the same extent and rate as we have reported in bovine aortic endothelial cells (Hsu, Lee et al. 2009, Lee, Haase et al. 2010).

The dependence of alignment on cyclic stretch frequency is consistent with previous measurements using U2OS cells and endothelial cells on fibronectin-adsorbed silicone rubber (Hsu, Lee et al. 2009, Hsu, Lee et al. 2010, Lee, Haase et al. 2010). In the present study, strain rate sensitivity was observed in cells cultured on collagen gels subjected to both steady and cyclic stretch patterns. Cyclic stretch at 0.01 and 1 Hz consisted of linear ramps (upward and downward) in strain of 0.2 and 20%/s, respectively. Cells subjected

to steady stretch at a ramp rate of 20%/s showed significantly more cell and SF alignment, as compared to cells subjected to steady stretch at a ramp rate of 0.2%/s (cf. Figs. 11E-F).Our theoretical model predicts that the strain rate-dependence is due to the active regulation of SF tension by actomyosin sliding (Kaunas and Deguchi 2011, Tondon, Hsu et al. 2012). Specifically, myosin II motors are predicted to translate along actin filaments in a direction that restores the forces acting on myosin heads to the values generated under static conditions. At high strain rates, we predict that myosin motors cannot respond quickly enough to regulate tension, while myosin can maintain tension nearly constant at low strain rates. We speculate that a similar mechanism regulates the strain-rate dependence observed for cells stretched on soft collagen gels.

Our results provide evidence that two mechanisms contribute to stretch-induced alignment on soft collagen gels. Prestretched collagen gels are expected to have anisotropic mechanical properties, with greater stiffness in the direction of stretch. The alignment of the cells and SFs along the direction of greater stiffness (cf. Fig. 11) is consistent with the alignment of cells on pillar arrays with anisotropic rigidity (Saez, Ghibaudo et al. 2007). Applying the stretch after the cells have spread on the collagen gel induced a greater extent of alignment, however (cf. Fig. 11). Since cells subjected to steady stretch are expected to experience both the stretch stimulus as well as the anisotropic rigidity of the gel, these results suggest that the act of stretching provides an additional contribution to the alignment response beyond changing the mechanical properties to the gel. Further, the effectiveness of the stretch stimulus depends on both the rate (cf. Fig. 11) and duration (cf. Fig. 12) of strain.

It is interesting to speculate on why the stretch stimulus is only effective on soft collagen gels, but not on collagen-coated sheets (cf. Fig. 11). Previous theoretical and experimental studies have indicated that cells are only sensitive to matrix stiffness within a limited range near the stiffness of the cell (Schwarz, Erdmann et al. 2006, Zemel, Rehfeldt et al. 2010). These models predict that cells cannot significantly deform substrates several orders of magnitude stiffer than the cells. Consistent with this prediction, cellular strains estimated from images of cells before and after a 10% step stretch indicate that cells deformed noticeably less on the soft collagen gels than on collagen-coated silicone rubber, suggesting that the cells are attenuating the stretching of the adjacent substrate (Supplemental Fig. B.3 and Table B.1). Perturbations in the stiffness of these substrates are therefore expected to be undetectable by the cells. Further, the silicone rubber substrate is elastic, hence does not stiffen upon stretching.

Cells in stretched 3-D collagen matrices are often elongated in parallel with the predominant alignment of collagen fibrils (Roby, Olsen et al. 2008). It has been suggested that the cells follow the collagen fibrils in a process termed contact guidance. In the present study, cells on collagen gels aligned along the direction of stretch without fibril alignment (cf. Fig. 9E), indicating that mechanical cues directly regulated cell and SF alignment.

Extracellular matrix geometry and topography at the nanoscale can impact cellular function (Guilak, Cohen et al. 2009, Zhang, Choi et al. 2013). Atomic force microscopy imaging of collagen-coated silicone sheets indicate a relatively uniform surface (Zhang, Choi et al. 2013). Collagen in fibrillar networks, on the other hand, is non-uniform with

relatively large spaces between fibrils for cell attachment, which is necessary for cell adhesion inside 3-D collagen gels. Gavara et al. (2008) observed that cells cultured on the surface of fibrillar collagen gels spread and displayed similar patterns of traction force distribution as cells seeded on polyacrylamide substrates coated with monomeric collagen, suggesting that the fibrillar nature of the collagen gels did not obviously change cell adhesive behavior on the surfaces of collagen gels vs. collagen-coated substrates Gavara, Roca-Cusachs et al. 2008). It is expected that the area density and configuration of cell binding sites on monomeric collagens adhering to silicone rubber will differ from that on fibrillar collagen. Thus, it would be advantageous to repeat these studies in the future using collagen-coated silicone rubber sheets with different Young's moduli to more directly assess the effects of stiffness.

A recent study by Pang et al. (2011) involving subjecting smooth muscle cells in 3-D collagen matrices showed an early cell response to external mechanical signals before they were fully spread out (Pang, Wang et al. 2011). Specifically, they observed initial cellular alignment within 2h of seeding cells and cells were completely aligned parallel to direction of stretch after 6h. Alignment of collagen fibrils along the stretch direction was only observed at 6h and was localized to the front of cell protrusions and attributed to the observed migration of cells parallel to the direction of stretch. In the system used Pang et al (Pang, Wang et al. 2011), the collagen hydrogel is only anchored at two ends, which generally leads to fibril alignment even in the absence of stretching due forces generated by contractile cells (Bellows, Melcher et al. 1982). Our results suggest that cells respond to both stretch-induced changes in stiffness and the stretch itself as part of

the initial response that occurs before any significant collagen remodeling has occurred. Further, the collagen hydrogels in our system were attached to stretch chamber on all sides other than the top free surface, which is expected to constrain any collagen remodeling that may occur at later times.

Our results indicate that stretch-induced SF alignment on soft collagen gels is dependent on MLCK, but not Rho-kinase. Rho-kinase and MLCK regulate central and peripheral SF populations, respectively (Tanner, Boudreau et al. 2010). SFs in cells stretched on collagen-coated silicone rubber contained central and peripheral populations of stress fibers, while mainly peripheral stress fibers were observed in cells on collagen gels (cf. Fig. 9). We have previously shown that cyclic uniaxial stretch induces the formation of actin fibers oriented parallel to the direction of stretch in cells treated with inhibitors of the Rho GTPase pathway and MLCK (Kaunas, Nguyen et al. 2005, Lee, Haase et al. 2010). In the present study with cells on collagen gels, cyclic stretch-induced actin fiber alignment parallel to the stretch direction was still observed upon Rho-kinase inhibition, but no alignment was observed upon MLCK inhibition (cf. Fig.13). We observed that ML7 treatment led to complete attenuation of SFs, while some actin bundles were observed in cells treated with Y27632 and these were oriented in the direction of stretch. Further, these actin bundles were located at the cell periphery, consistent with previous reports that Y27632 only inhibits SFs located centrally, while ML7 inhibits SFs located at the cell periphery (Katoh, Kano et al. 2001, Kaunas, Nguyen et al. 2005, Lee, Haase et al. 2010).

Our findings shed new light on experimental and theoretical observations by other groups on cells stretched on soft 2D and 3D substrates (Krishnan, Park et al. 2009, Lee, Nekouzadeh et al. 2012, Ronan, Deshpande et al. 2013). Consistent with our predictions, the theoretical models of McGarry and Deshpande (Deshpande, McMeeking et al. 2006, Ronan, Deshpande et al. 2013) predict that softer substrate do not provide sufficient tension for SF persistence, causing dissociation of SFs, while cells on a stiffer substrate are predicted to contain large amount of dominant SFs under optimal tension. Genin and Elson (Lee, Nekouzadeh et al. 2012) showed that SFs in cells inside a 3D engineered tissue construct undergo retraction and subsequent reinforcement when subjected to stretch. Retraction response was observed for SFs in all direction, while reinforcement response was observed only in the stretch direction. The reinforcement response and alignment of SFs in stretch direction is consistent with our observation on 2D soft collagen gels. Krishnan et al. (2009) and Trepat et al. (2007) also reported cytoskeletal fluidization and reinforcement in cells subjected to stretch on soft polyacrylamide substrates (Trepat, Deng et al. 2007, Krishnan, Park et al. 2009). However, we did not observe an obvious fluidization or retraction in SFs after a step increase in stretch in cells expressing GFP-actin (cf. Fig. 13).

Recent studies by Quinlan et al. (2011) and Faust et al. (2011) report that cells have attenuated alignment in response to stretch on soft polyacrylamide and soft silicone rubber substrates, respectively. Faust et al. (2011) subjected cells to stretch at frequencies in the mHz range. In our current and past studies, we observed no alignment when stretching cells at a frequency of 10 mHz. Thus we predict that low strain rate due

to low frequency cyclic stretching is not sufficient to induce alignment. Furthermore, polyacrylamide and silicone rubber are elastic, hence do not stiffen upon stretching. In the absence of the anisotropic changes in substrate rigidity, stretch alone may not be sufficient to stimulate alignment. Moreover, Quinlan et al. and Faust et al. used different cells type (porcine aortic valve interstitial cells and primary human umbilical cord fibroblasts, respectively) than we did, which may also contribute to the apparent discrepancies.

III.D Conclusion

In summary, our results demonstrate that stretch-induced cell and SF alignment are highly dependent on the mechanical properties of the collagen matrix upon which cells are cultured. Recent experiments employing high-resolution traction force microscopy on polyacrylamide substrates indicate that focal adhesions individually sample the substrate rigidity and that FAK/phosphopaxillin/vinculin signaling defines the rigidity range over which cells migrate toward regions of higher rigidity (Plotnikov, Pasapera et al. 2012). On the other hand, experiments performed on elastic pillar arrays interpreted with a phenomenological model based on active gel theory suggest that rigidity-sensing is mediated by a large-scale mechanism originating in the cytoskeleton rather than local sensing at the level of focal adhesions (Trichet, Le Digabel et al. 2012). While our results are consistent with a large-scale mechanism involving the actin cytoskeleton and myosin motor proteins, we cannot rule out the role of focal adhesion proteins.

CHAPTER IV

A NOVEL HMATRIX COATED POLY-ETHER-ETHER-KETONE (PEEK) BASED MOUSE FEMORAL SEGMENTAL DEFECT FIXATION DEVICE

IV.A Introduction

Bone is a dynamic tissue that undergoes constant remodeling. Bone remodeling is a physiological process in which old bone is degraded by osteoclasts and subsequently replaced by new bone formed by osteoblasts. While bone has a remarkable capacity for regeneration, critical sized bone defects are don't heal completely due to the extent of the trauma, disease, or age of the patient (Boden 2000, Green, Lubahn et al. 2005) In fact, one tenth of all limb bone fractures fail to heal. Autologous bone grafting procedures are effective, but limited availability of graft material and additional surgery requirement are some of the drawbacks (Rihn, Kirkpatrick et al. 2010).

Dr. Gregory's lab addressed this limitation by improving the osteogenic capacity of human mesenchymal stem cells (hMSC) by accelerating the canonical wingless (cWnt) pathway. In a recent study, they demonstrated that when peroxisome proliferator activated receptor- gamma (PPAR) is inhibited by exposure to the small molecule GW9662, negative cross-talk on the cWnt pathway is relaxed resulting in the establishment of a pro-osteogenic hMSC phenotype (OEhMSCs) (Krause and Gregory 2012). These OEhMSCs secreted a large amount of matrix (hMatrix) containing a complex mixture of collagen molecules that mimics the composition of anabolic bone

tissue. When hMatrix is co-administered with OEhMSCs, the cell-matrix composite has a unique capacity for rapid repair of experimental bone defects in rodents (Zeitouni, Krause et al. 2012).

Dr. Gregory's lab has developed a novel device that permits fixation of the mouse femur after removal of a 3 mm section of the bone. After the establishment of the defect and installation of the device, the mice will be mobile with full limb functionality. We synthesized the device from poly-ether-ether-ketone (PEEK), a plastic used commonly in clinical surgical implants because it is safe, durable, and most importantly, permits x-ray imaging without interference - a drawback of all metal implants. However, the poor ability of PEEK to support cellular adhesion is unfavorable for many applications where tissue integration is desired (Kurtz and Devine 2007). In order to overcome this limitation, we developed a facile technique to modify PEEK surface to allow covalent attachment of hMatrix, with a view to enhance osteointegration. Modification of polymer PEEK surface was achieved by the generation of pendant primary amino groups using a diamine. Covalent bonding of hMatrix is achieved by formation of amide bond between hMatrix peptides and PEEK surface using water-soluble 1-ethyl-3-[3-dimethylaminopropyl]-carbodiimide hydrochloride (EDAC).

IV.B Methodology and Results

PEEK sample preparation and hMatrix crosslinking

Samples of desired dimensions were cut from medical grade PEEK rods (VESTAKEEP®) and cleaned with isopropanol and water. These PEEK samples were

immersed in neat ethylene diamine (EDA) and treated for a period of 3h at 120∘C, followed by thorough washing with water and isopropanol. The reaction was carried out using an air cooled condenser system inside a fume hood. Silicone oil bath was used to heat the EDA solution. Covalent bonding of hMatrix was achieved by using 1-ethyl-3-[3-dimethylaminopropyl]-carbodiimide hydrochloride (EDAC), a water soluble carbodiimide (Fig. 14). Modified PEEK samples were incubated with EDAC and hMatrix at room temperature for 3 hours. The dried samples were UV sterilized for 1h and washed with α-MEM before seeding cells. hMatrix adhesion was qualitatively determined through scanning electron microscopy analysis of samples. Scanning electron microscopy demonstrated 3-dimensional fibril aggregates of hMatrix attached to the PEEK samples (Fig. 15A).

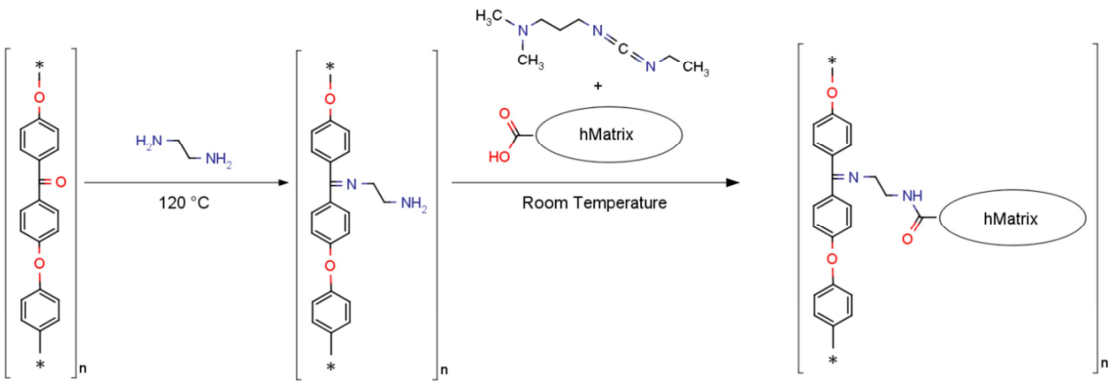

Figure 14. Reaction scheme for the cell-adhesive modification of PEEK. hMatrix components can be covalently attached to modified PEEK surface achieved by the generation of pendant primary amino groups using ethylenediamine followed by carboiimide based crosslinking approach.

Assessment of hMSCs adhesion and proliferation on modified PEEK

hMSCs culture on bare and hMatrix-coated PEEK was performed for the initial attachment phase and for a 1-week period. Briefly, the PEEK samples were sterilized and washed with α-MEM before seeding cells. hMSCs were allowed to grow for a 1-week period. PEEK exhibits a strong autofluorescence which prohibited the use of standard fluorescent dyes for cell staining and imaging. To circumvent this limitation we used thin optically clear sheets of PEEK to image cells (Fig. 15 B). We also performed Scanning Electron Microscopy (SEM) to analyze cell adhesion on PEEK segmental defect implants. After culture, the samples were dried using methanol and fixed using 4% glutraldehyde as described previously (Parameswaran and Verma 2011). While untreated PEEK showed almost negligible colonization by hMSCs even after 1 week, the hMatix-coated PEEK film and samples exhibited excellent cellular adhesion and proliferation (Fig. 15 C &D). These results, obtained in vitro, need to be further elucidated in animal experiments.

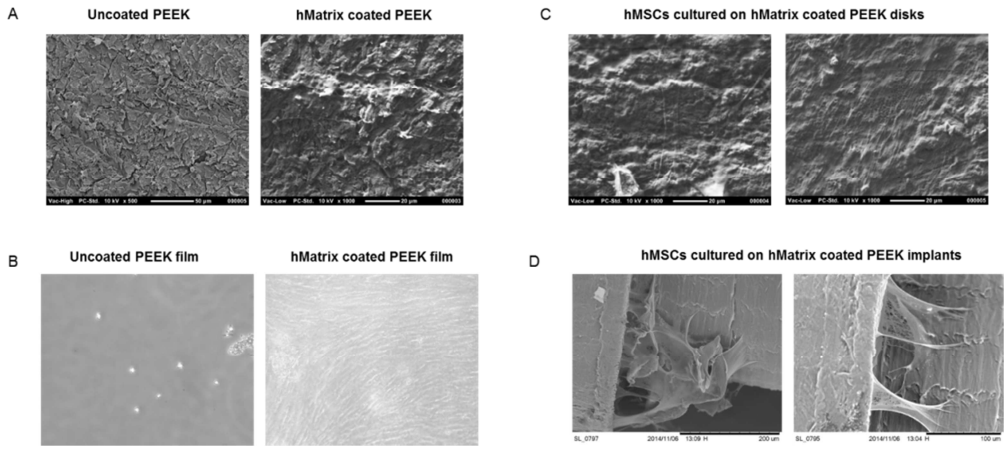

Figure 15. Crosslinking of hMatrix to PEEK surface and hMSCs culture. (A) Scanning electron micrograph of uncoated and hMatrix coated PEEK disks. **(B)** DIC images of hMSCs cultured on uncoated and hMatrix coated optically clear PEEK films. **(C & D)** Scanning electron micrograph of hMSCs cultured on hMatrix coated PEEK disks (C) and hMatrix coated PEEK segmental defects implant (D).

IV.C Discussion

Our results demonstrate that we have developed a facile technique for the wet-chemical modification of PEEK surface and coating the modified PEEK surface with anabolic hMatrix. Plasma treatment and various photochemical routes have been explored to enhance the cell adhesion properties of PEEK polymer. In contrast to photochemical and plasma technologies which suffer from limitations regarding the treatment of geometrically complex structures, liquid based modifications are mostly feasible. In addition, plasma treatment only provides a temporary enhancement in cell adhesion (Briem, Strametz et al. 2005, Becker, Lorenz et al. 2013). In this work, we utilized

chemical reduction with a diamine for the formation of a Schiff base (ketamine) between the keto groups of PEEK and one amino portion of ethylenediamine. These free amine groups then served to conjugate carboxyl containing peptides using, an amine bond. We also use this method to covalently coat peptides on the surface of plasma modified polystyrene.

Bare PEEK does not support cellular attachment. Whereas, hMatrix coated PEEK showed excellent cell adhesion and proliferation (Fig. 15 B - D). As shown in precious studies, hMatrix mimics the composition of anabolic bone tissue (Zeitouni, Krause et al. 2012). As a possible substitute for titanium, PEEK matches more closely the mechanical properties of bone. In order to achieve better osteointegration of PEEK implants, we coated the PEEK surface with hMatrix and tested attachment and proliferation of hMSCs. These results, obtained in vitro, may be further elucidated in animal experiments under realistic in vivo conditions.

IV.D Conclusion

The increasing utilization of PEEK as orthopedic implants, requires methods to enhance the cellular adhesion on PEEK surface. A wet-chemical technique was developed that is based upon a ketamine-based activation of the PEEK surface in combination with covalent attachment of hMatrix using carbodiimide chemistry. This method, may serve as a promising approach to enhance the osteo-integration and performance of PEEK implants.

CHAPTER V

3-D METHOD TO EXAMINE BONE TUMOR AND HOST TISSUE INTERACTIONS USING MICRO-GRAVITY BIOREACTOR

V.A Introduction

Malignant bone disease (MBD) can occur by metastasis (e.g. from breast and prostate) or as a result of a primary bone tumor (e.g. osteosarcoma). When tumors establish in bone, catastrophic tissue damage occurs as a result of accelerated bone destruction and inhibition of repair. The resultant so called osteolytic lesions (OL) can cause pain and fractures, but more importantly, they provide an ideal niche for tumor propagation. Tumors maintain this microenvironment by secreting Wnt inhibitors (WIs) that prevents hMSCs from differentiating into osteoblasts. Tumor-derived secretion of cWnt-antagonist Dickkopf-1 (Dkk-1) is known to cause bone destruction, inhibition of repair and promote bone metastasis (Tian, Zhan et al. 2003, Gregory, Gunn et al. 2005). Recent study by Krause et al. (2014), showed that mouse osteosarcoma cells engineered to express Dkk-1 (MOSJ-Dkk1) not only reduced the capacity for osteogenic differentiation *in vitro* and *in vivo*, but also increased proliferation, resistance to metabolic stress and the capacity for osteolytic tumorigenesis *in vivo* . To discover ways to inhibit the activity of WIs, it is necessary to mimic the interactions between bone tumor cells and MSCs in an experimentally accessible system that sufficiently recapitulates the *in vivo* microenvironment.

Although convenient, monolayer co-culture systems do not accurately replicate 3D tissue and are poor predictors of drug efficacy *in vivo.* It's now well understood that physiological 3D growth conditions allowing unrestricted cell- cell interactions are important for defining the biology of cancer cells and tissue, including tumor formation and progression (Kwon, Devarakonda et al. 2008, Barzegari and Saei 2012). In contrast to physiological growth conditions, monolayer culture involves cells interaction with stiff, flat surface and has limited cell–cell interconnectedness.

Cells exposed to microgravity culture conditions are extensively affected by the physical changes that occur under these unique condition, which include lack of gravity-dependent convection, no hydrodynamic shear and sedimentation (Todd 1989, Todd 1991, Unsworth and Lelkes 1998, Hammond and Hammond 2001). These changes in physical environment of the cells results in their ability to coalesce and form complex multicellular aggregates and organoids. (Freed, Langer et al. 1997, Unsworth and Lelkes 1998). NASA (National Aeronautics and Space Administration) developed a the rotating wall vessel (RWV) bioreactor to generate simulated microgravity condition on earth, which allowed the ability to achieve unrestricted 3D growth in suspension on Earth, similar to that observed in microgravity. (Tsao, Goodwin et al. 1992, Goodwin, Prewett et al. 1993). The rotating wall vessel (RWV) is an excellent tool for this purpose as it permits the growth of 3D tissue constructs while facilitating excellent fluid and gas exchange. Indeed, it is not uncommon to generate viable constructs upwards of 3 mm in diameter compared to the upper limit of approximately 1 mm in conventional bioreactors.

As discussed in Chapter III, pro-osteogenic MSCs (osteogenically enhanced hMSCs, OEhMSCs) secretes matrix that resembles the composition of anabolic bone tissue (hMatrix). When co-administered with OEhMSCs, the cell-matrix composite has a unique capacity for rapid repair of experimental bone defects in rodents (Zeitouni, Krause et al. 2012). Using a variation of the technique developed in chapter III, we covalently linked hMatrix to polystyrene microspheres to mimic the biochemical and mechanical microenvironment of anabolic bone.

To generate an experimental platform for the study of bone-tumor interactions, we established an in vitro system where bone tumor cells are co-cultured with OEhMSCs in a RWV. The hMSCs and tumor cells were seeded separately onto novel hMatrix coated polystyrene microspheres that mimic the surface of anabolic bone tissue. While RWVs have been used before to examine tumor-stroma interactions, we incorporated following innovative improvements:

i) novel microspheres for optimal biochemical and mechanical mimicry of mineralized bone matrix (hMatrix coated polystyrene spheres);
ii) a novel source of primary human osteoprogenitors (OEhMSCs);
iii) a well-characterized osteolytic bone tumor cell line with a genetically identical nonosteolytic control (MOSJ-Dkk1 and MOSJ-pLenti cells).

V.B Methodology and Results

hMatrix harvesting and crosslinking to spheres

hMatrix was harvested from OEhMSC monolayers cultured for 8 days in α-minimal-essential-media containing 20% fetal bovine serum, 50 μg/ml ascorbic acid, 5 mM β-glycerol phosphate and 10 μM GW9662. OEhMSC monolayers were washed in PBS and frozen at -80°C to disrupt cell membranes, thawed, and scraped from the culture plate. Recovered cells and matrix were pelleted by centrifugation and suspended in lysis buffer (0.1% Triton X100, 1 mM $MgCl_2$, 10 μg/ml DNAse I, 10 mg/ml RNAse A in PBS) with shaking at 60 rpm for 4h at 37°C and an additional 16h in the presence of 0.125% (v/v) trypsin. The remaining hMatrix was recovered by centrifugation and washed in distilled water and chloroform. Finally, hMatrix was rinsed in acetone and air-dried under sterile conditions. At time of use, the hMatrix was reconstituted in 2% (v/v) acetic acid at a concentration of 1 mg/ml. By this method, approximately 1 mg of material can be generated per cm^2 of monolayer.

We used 1-Ethyl-3-(3-dimethylaminopropyl)carbodiimide (EDAC) to crosslink hMatrix to the polystyrene spheres (Corning) using a modified approach described previously (Macklis, Sidman et al. 1985). Plasma treatment of polystyrene creates reactive carboxyl groups on the surface of the untreated beads to allow crosslinking. Commercial plasma treated polystyrene beads available from Corning were used. Briefly, these plasma treated polystyrene microspheres were mixed with an excess solution of EDC and hMatrix for 3h on a shake plate at room temperature. The microspheres were washed

twice with PBS and air dried. The dried spheres were UV sterilized and washed with α-MEM before seeding cells (Fig.16 A).

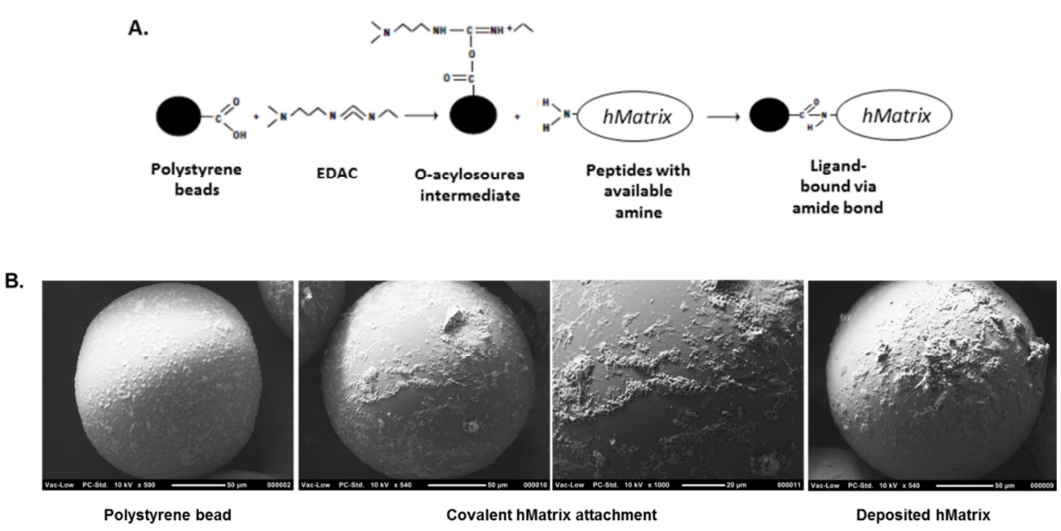

Figure 16. hMatrix harvesting and crosslinking to spheres. (A) hMatrix components can be covalently attached to polystyrene beads using carbodiimide-based crosslinking approach. **(B)** Electron Microscopy of a polystyrene bead before (left), after covalent hMatrix attachment (middle) and with hMSCs deposited hMatrx (Right).

Assessment of hMatrix adhesion to spheres

hMatrix adhesion was qualitatively determined through immunocytochemistry and scanning electron microscopy analysis of the samples. Scanning electron microscopy demonstrated that high molecular mass aggregates of hMatrix attach to the beads creating a complex 3-dimensional topology (Fig. 16 B). hMatrix is a complex mixture of

multiple proteins (Zeitouni, Krause et al. 2012), with collagen type I is a major component. The coated microspheres were immunostained with a mouse monoclonal anti-human collagen type I antibody followed by a secondary anti-mouse antibody conjugated to a fluorophore (e.g. Alexa 488). Immunocytochemical detection of collagen I, confirmed the identity of the attached structures (Fig. 17 A).

Direct hMatrix deposition by hMSCs

We have successfully devised a method to decellularize the polystyrene microspheres without disrupting hMatrix deposited by the OEhMSCs. Briefly, OEhMSCs were seeded directly onto the enhanced plasma treated polystyrene microspheres and grown for 8 days in osteogenic base medium (α-minimal-essential-media supplemented with 20% fetal bovine serum, 50 μg/ml ascorbic acid and 5 mM β-glycerol phosphate) containing 10 μM GW9662BM within a RWV. Vessel contents were then extracted, centrifuged, washed with PBS, and re-suspended in 0.2% ammonium hydroxide solution for 10 minutes to remove cells. To remove any residual DNA, the samples were then suspended in PBS containing 0.1% v/v Triton X100, 1 mM $MgCl_2$, and 1 U/mL DNAse I and placed in an incubator at 37 °C for 2 hours. hMatrix adhesion was qualitatively determined through scanning electron microscopy analysis of samples as described above. The results indicate that hMatrix applied to the surface of polystyrene beads via direct depositing by OEhMSC is similar to that achieved by covalent grafting of reconstituted hMatrix (Fig 16 B).

hMSCs culture in the Rotating Wall Vessel

We utilized an 8-vessel bioreactor system (Synthecon, model RCCS-8DQ), with 10 mL disposable high aspect ratio vessels. We used microsphere with a total surface area equivalent to 55cm^2 and with approximately 2 million OEhMSCs per vessel at the start of culture. Rotation rates were established by visual observation of the free-fall rates of the aggregates in suspension and adjusted as required to maintain a gentle free-fall, while limiting the wall impacts of the aggregates. Cultures were allowed to proceed in the presence of osteogenic base media supplemented with glucose if necessary. At the conclusion of the culture period, cell – spheres aggregates were recovered and the number of viable cells was enumerated by qRT-PCR for GAPDH.

MOSJ-Dkk1 and MOSJ-pLenti culture

We used two related murine bone tumor cell lines generated by the Gregory's lab (Krause, Ryan et al. 2014). The cell lines were perfectly suited for this work because they are genetically identical with the exception that one line constitutively expresses human Dkk-1, a highly potent Wnt inhibitor and inhibitor of osteogenesis (MOSJ-Dkk1) and the other has negligible inherent osteolytic activity (MOSJ-pLenti). Therefore, MOSJ-Dkk1 cells are highly osteolytic whereas control cells are somewhat osteogenic *in vivo*. Microsphere culture of osteosarcoma cell lines MOSJ-Dkk1 and MOSJ-pLenti were optimized in a similar manner to the OEhMSCs. While we have no definitive release criteria for the MOSJ cells, preliminary data by Dr. Gregory's lab indicates that while MOSJ-pLenti control cells differentiate *in vitro* and *in vivo* into osteoblast-like

cells, MOSJ-Dkk1 cells are highly proliferative with the complete absence of osteogenic potential. We expect that our co-culture results will reflect these observations.

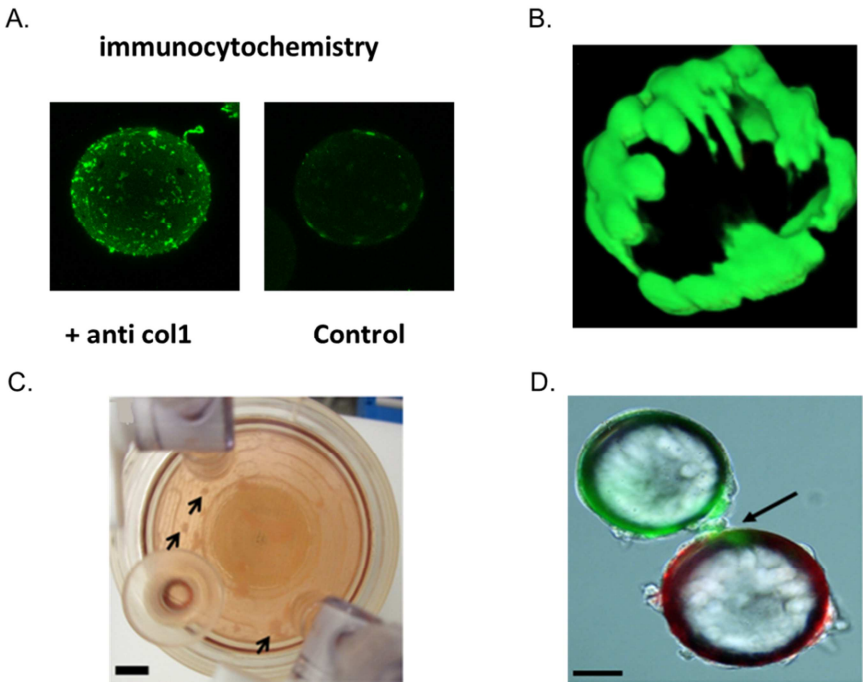

Figure 17. RWV Bioreactor culture. (A) Collagen I, a major constituent of hMatrix is detected by immunocytochemistry (bar = 50μm). **(B)** Example of a 3D reconstruction of calcein AM labelled OEhMSCs-microsphere live cell confocal microscopy. **(C)** Photograph of RWV showing loosely aggregated cell-laden microspheres containing OEhMSCs and MOSJ-DKK1 cells *(arrowed)* (bar = 10mm). **(D)** High power micrograph of an OEhMSCs-laden sphere (green) potentially passing a cell to MOSJ DKK1- laden sphere (red) suggesting MSC-tumor transfer *(arrowed)* (bar = 50μm).

OEhMSC-laden and MOSJ -laden spheres co-culture in RWV

After establishing the optimal parameters for culture of OEhMSC-laden and MOSJ-laden microspheres in RWV, we performed the co-culture experiments with OEhMSCs and MOSJ-Dkk1 osteolytic osteosarcoma cells or MOSJ-pLenti osteogenic osteosarcoma cells in an effort to mimic osteolytic and osteogenic bone-tumor microenvironments. For these experiments, 2 million OEhMSCs were attached to hMatrix-coated beads and then cultured for 2 days in a RWV. Thereafter, beads laden with MOSJ-Dkk1 or MOSJ-pLenti cells were added to the cultures at a ratio of approximately 5 OEhMSC beads: 1 MOSJ bead. Cultures were allowed to proceed for 2, 4 and 8 days before recovery and analysis. Over the 8 day period, the co-cultures and OEhMSC-alone controls generated cell-aggregates of up to 5 mm in diameter but could be gently dissociated upon recovery (Fig. 17 C).

Assessment of cell growth and osteogenesis in OEhMSCs and MOSJ co-culture

We performed osteogenic assays on the recovered aggregates from the RWV cultures to examine whether MOSJ-Dkk1 cells had the expected effect of inhibiting osteogenesis by OEhMSCs, when compared to OEhMSC-alone controls and co-cultures with osteogenic MOSJ-pLenti cells. We recovered media and mRNA to perform ELISA and quantitative RT-PCR (qRT-PCR) respectively. We measured the transcription of collagen I, osteogenic transcription factor runx2, bone morphogenic protein 2 (BMP2), and the cWnt signaling marker axin 2 by qRT-PCR.

To determine the numbers of OEhMSCs and MOSJ cells in the cultures, we employed species-specific qRT-PCR for GAPDH because OEhMSCs are human and MOSJ cells are murine (Fig. 18 A - D). The numbers of OEhMSCs remained constant at approximately 1.5 - 2 $x10^6$ cells when cultured in the absence of MOSJ cells, but dropped during co-culture by up to 75% (Fig. 18 C). This is presumably due to the accumulation of MOSJ- DKK1 cells in the culture (Fig. 18 D). Interestingly, MOSJ-pLenti cells caused an equivalent drop in OEhMSCs, yet did not divide as quickly as MOSJ-Dkk1 cells. The reason for this observation is unclear, but it's possible that MOSJ-pLenti cells take up more surface area than MOSJ-Dkk1 cells, or MOSJ-pLenti cells directly inhibit proliferation.

As expected, MOSJ-Dkk1 human suppressed OPG secretion (Fig. 18 E) when compared to OEhMSC- alone cultures and MOSJ-pLenti cells. In the RWV, we also observed that MOSJ-pLenti cells were potentially osteogenic in that they upregulated the secretion of human OPG by OEhMSCs (Fig. 18 E). We then measured the transcription of collagen I, osteogenic transcription factor runx2, bone morphogenic protein 2 (BMP2), and the cWnt signaling marker axin 2 by qRT-PCR (Fig. 19). Surprisingly, co-culture with both forms of MOS-J cell caused a reduction in the steady-state levels of collagen I mRNA at day 4 when compared to OEhMSC alone controls, but levels were lowest in MOSJ-Dkk1 co-cultures (Fig. 19 A). However at day 8, significant reduction in expression of collagen I was only observed for MOSJ-Dkk1 co-cultures indicating a reduction in hMSCs osteogenesis by DKK-1.

In the case of BMP2 and runx2 transcription, MOSJ-Dkk1 cells caused a reduction of transcription whereas MOSJ-pLenti cells caused no significant changes in transcription (Fig. 19 B&C). The levels were lowest at day 8 in MOSJ-Dkk1 co-cultures. Axin2 mRNA was also reduced in MOSJ-Dkk1 co-cultures but was slightly upregulated upon co-culture with MOSJ-pLenti cells at day 4 (Fig. 19 D).

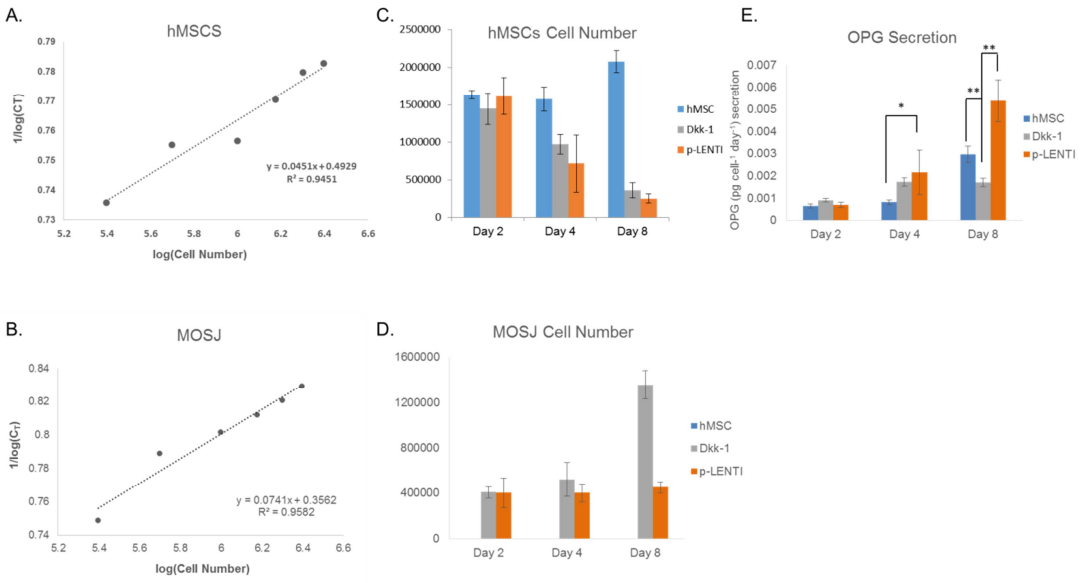

Figure 18. Osteogenic activity of OEhMSCs cultured in the presence and absence of MOSJ-DKK1 and MOSJ-pLenti cells in an RWV. Species-specific measurement of OEhMSCs by qRT-PCR for human GAPDH mRNA **(A)**. Species-specific measurement of MOSJ-DKK1 and MOSJ-pLenti by qRT-PCR for murine GAPDH mRNA **(B)**.The number of OEhMSCs present after 2, 4, and 8 days of culture in RWV **(C)**. The number of MOSJ-Dkk1 and MOSJ-pLenti present after 2, 4, and 8 days of culture in RWV **(D)**. Secretion of human-OPG as measured by ELISA **(E).** Significant differences between groups were determined by ANOVA followed by Student-Neuman–Keuls post-hoc multiple comparison testing P<0.01*, <0.05**.

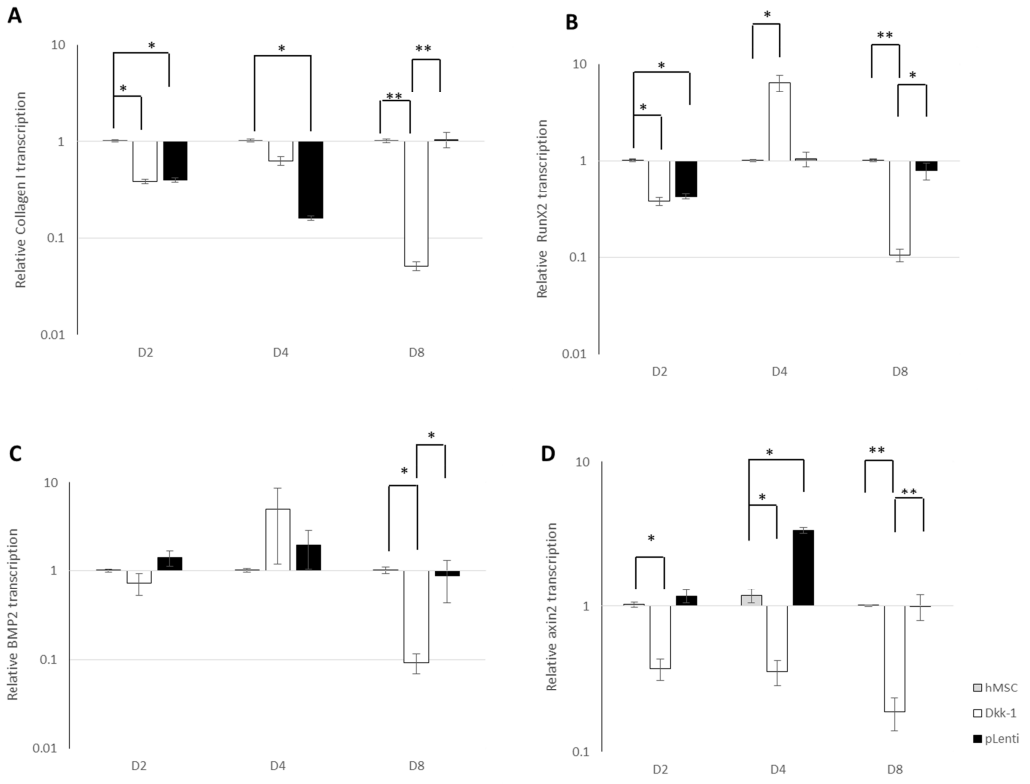

Figure 19. qRT-PCR assays of osteogenic and Wnt-responsive transcripts. Human-specific qRT-PCR was performed for osteogenic transcripts collagen I (A), osteogenic transcription factor runx2 (B), osteogenic ligand BMP2 (C) and Wnt-responsive transcript axin2 (D). Values are presented as transcription relative to OEhMSC-only control culture where the expression level is set to 1**. Statistics:** Significant differences between groups were determined by ANOVA followed by Student-Neuman–Keuls post-hoc multiple comparison testing P<0.05*, <0.01**.

Dr. Gregory's lab performed direct monolayer co-culture for comparison. They utilized direct fluorescence to determine the numbers of OEhMSCs and MOSJ cells through their expression of GFP and RFP respectively. While the data for the monolayer controls

were qualitatively equivalent to the RWV data, the normalized values for OPG secretion were consistently 3- to 5-fold higher in monolayer cultures when compared to those performed in the RWV. It is possible that this observation might be due to reduced gravitational influence but we have not excluded the possibility of modest shear effects due to the motion of the RWV. We expect that experiments in true microgravity will address this question.

Ground based static experiments

Upon optimization of the RWV culture system, we performed a series of static culture experiments utilizing culture equipment compatible with the International Space Station (ISS) laboratory. We will use the data from these experiments to serve as a control for co-cultures planned to be performed on the ISS. For this purpose, we utilized Teflon bags (VueLife® 32-C, American Fluorsel) with 10 mL culture volume and hung horizontally in a conventional incubator with no agitation. As expected, both the OEhMSCs alone and MOSJ co-culture performed poorly in the Teflon bags under normal gravity conditions (Fig. 20 A).The cell aggregates settled down and formed loosely associated sheet like structures that dissociated on lifting the bags.

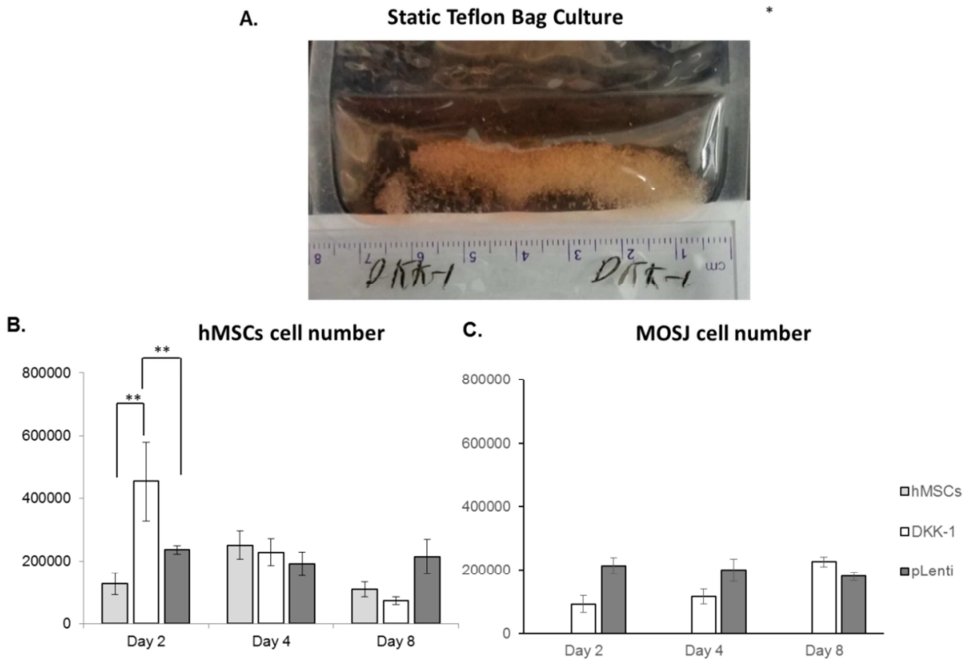

Figure 20. Translation to space-based experiments. Co-culture experiment performed using Teflon bags under normal microgravity conditions (**A**). The number of OEhMSCs present after 2, 4, and 8 days of culture in teflon bag **(B)**. The number of MOSJ-Dkk1 and MOSJ-pLenti present after 2, 4, and 8 days of culture in teflon bag **(C)**. **Statistics:** Same as figure 18.

V.C Discussion

Our results demonstrate that we have developed and optimized a novel in-vitro platform for the study of bone-tumor interactions under simulated microgravity conditions. Although convenient, monolayer co-culture systems don't accurately replicate 3D tissue and are poor predictors of drug efficacy in vivo (Hoffman 1994, Unsworth and Lelkes 1998, Grimm, Wehland et al. 2014). On the other hand, in vivo assays based on implantation of tumors in rodents are often complex, laborious and in some cases,

technically challenging (Campbell, Merkel et al. 2012, Kretschmann and Welm 2012, van der Horst and van der Pluijm 2012). To the best of our knowledge, this is the first 3D co-culture model of malignant bone disease (MBD) mimicking the interactions between osteolytic bone tumor and host tissue.

Our 3D co-culture model consists of osteogenically enhanced MSCs (OEhMSCs) cultured with osteolytic bone tumor (MOSJ - DKK1) cells within a rotating wall vessel bioreactor. The hMatrix coated polystyrene microspheres mimics the biochemical and mechanical microenvironment of mineralized bone matrix (Yeung, Georges et al. 2005, Zeitouni, Krause et al. 2012). We used a well-characterized osteolytic bone tumor cell line (MOSJ- DKK1) which constitutively expresses human Dkk-1, which has been shown to enhance proliferation and survival of tumor cells in osteolytic lesions (Krause, Ryan et al. 2014). In addition, the addition of PPARγ inhibitor GW9662 to culture relaxes the negative cross-talk on the canonical Wnt pathway, establishing a pro-osteogenic MSC phenotype observed in native human bone tissues (Krause, Harris et al. 2010).

From our co-culture model, MSC and tumor cells interactions were apparent. We observed that most cell-sphere aggregates harbored both OEhMSCs and MOSJ tumor cells suggesting extensive transfer during co-culture (Fig 17 D) (Gregory's lab data). Previous studies indicate that in the bone marrow, MSC play an important pro-tumorigenic role by promoting osteolytic bone metastasis and tumor cell proliferation. We predict that tumor-homing potential may be due to the fact that as MSCs undergo osteogenesis they produce chemoattractant proteins like SDF-1 and MCP-1 which are

very potent chemo attractants for tumor cells (Urashima, Chen et al. 1997, Burger and Kipps 2002, Molloy, Martin et al. 2009).

As expected, we saw a reduction in osteogenic potential of OEMSCs in our co-culture model which is consistent with previous in-vivo and in-vitro observations. We observed a significant reduction in expression of osteogenic markers collagen I, runx2 and BMP2 in MSCs co-cultured with MOSJ –DKK1 cells as compared to MSC alone culture and control MOSJ –pLenti co-culture. This is consistent with recent in-vivo study by Dr. Gregory's lab, where they observed that MOSJ-Dkk1 injected homozygous nude mouse developed large tumor nodules in the soft tissue with significant lytic bone destruction. Whereas, only isolated osteochondral tumor nodules were observed in soft tissue in mice injected with control MOSJ-pLenti cells. In addition, minimal involvement with host bone was observed (Krause, Ryan et al. 2014). In addition, MOSJ-Dkk1 cells inhibited human OPG secretion (Fig. 18 E) when compared to MSCs alone and control MOSJ-pLenti co-culture.

The inhibition of MSC osteogenesis in our co- culture model is similar to osteo-inhibition seen in osteolytic lesions which prevents bone repair and may encourage metastasis (Glass and Karsenty 2007, Pinzone, Hall et al. 2009). It is now well established that cWnt signaling and DKK1 are involved in bone metastases and formation of osteolytic lesions. Tumor derived secretion of DKK1 has been shown to block maturation of osteoblasts and formation of mineralized matrix by antagonizing the cWnt pathway in osteolytic bone lesions (Mukhopadhyay, Shtrom et al. 2001, Grotewold and Ruther 2002, Zuzarte-Luis, Montero et al. 2004, Glass and Karsenty

2007). Recent studies have shown that DKK1 contributes to the osteolytic phenotype by shifting the expression of OPG and receptor activator of NF-κB ligand (RANKL), which are positively and negatively regulated by canonical Wnt signaling in osteoblasts, respectively (Qiang, Chen et al. 2008). We observed a decrease in mRNA expression levels of axin2 a marker of cWnt pathway activity suggesting a downregulation of cWnt pathway.

Osteoclastic bone resorption inhibiting drugs, such as bisphosphonates (zoledronic acid and ibandronate) or RANKL antibodies (Denosumanb) are the current standard of care for patients with bone metastases (Rose and Siegel 2010). There is emerging data that these anti-resorptive agents can also have direct anti-tumor effects. However, 30–50% of patients on these therapies develop new bone metastases and disease progression, emphasizing the need for new therapies (Roodman 2004). Although chemotherapy-induced tumor reduction and bone resorption inhibitors are effective at halting osteolytic lesions, there is no compensatory osteoblastic or anabolic response. Recently there has been an increased interest in therapeutic targeting of osteogenesis inhibitors and several agents with bone anabolic properties are currently undergoing clinical evaluation, including BHQ880 (DKK-1 neutralizing antibody). Our model provides an excellent medium throughput model for discovery and analysis of new drug targeting bone anabolic targets for the repair of OLs and the destruction of drug-sensitive tumor cells.

One unique opportunity with this study is the possibility of transferring concept and experimental co-culture model of malignant bone disease to space station in the future, where reduced gravity conditions exists naturally. In a previous study conducted on

International space station, Wang et al. (2005) observed a significant difference in the sizes of the aggregates between experiment conducted using RWV and those conducted in space (Wang, Xu et al. 2005). They observed golf-ball size prostate tumor organoids within 6 days on experiment performed in space, whereas in the same period aggregates of only 3–5 mm in diameter were formed under stimulated microgravity condition using RWV. There was a remarkable difference in the sizes of the aggregates. This is consistent with the size of the aggregates we observed in OEhMSCs alone and OEhMSCs-MOSJ co-culture in RWV. The planned space based experiment will offer new insights into the nature of the tumor- stroma interaction and allow us to understand the molecular steps underlying the co-evolution of cancer and stromal cells. These insights will be used to further improve our 3D co-culture model of MBD for future drug discovery.

The ground-based static experiments will provide the necessary data for successful translation to space. These experiments will guarantee comparability between those performed in the RWV, in Teflon bags at 1G and those performed in microgravity on the ISS. As expected in the static ground experiment the cell aggregates settled down and formed loosely associated sheet like structures that dissociated on lifting the bags. We predict these cultures suffered from suboptimal fluid and gas exchange as they sediment to the bottom of the bag. We do not expect this to be the case in microgravity, given previous observations from similar space-based experiments (Becker and Souza 2013), and we expect that the lack of sedimentation and constant gentle motion of the spheres

will result in excellent culture conditions that result in large accumulations of cells on the spheres

V.D Conclusion

Successful execution of these studies will lead to a range of new methods for the investigation of tumor-stem cell interactions without the limitations of 2D tissue culture or *in vivo* approaches. Furthermore, we expect that this approach will significantly accelerate drug research and discovery of new drugs for the repair of OLs and the destruction of drug-sensitive tumor cells.

The leading drug approved to reduce bone damage caused by cancer, Zometa, has taken $1288 million in total sales but it has substantial limitations and side effects. We believe that our proposed approach will substantially improve drug research in this field and generate interest from the pharmaceutical industry. Experiments of this type adapted for execution in space are also likely to substantially improve our understanding of tumor expansion and bone repair during long term exposure to micro-gravity.

CHAPTER VI

OVERALL DISCUSSION AND CONCLUSION*

Soluble messengers have been known to effect cellular behavior. In addition, cells interactions with chemical and physical interactions with non-soluble components of the ECM have been known to influence various cellular processes, including adhesion, migration and differentiation. Recently it has become increasingly clear that cytoskeletal tension plays a significant role in maintaining normal cell function through modulation of intracellular signaling and gene expressions (Kaunas, Usami et al. 2006, Hsu, Lee et al. 2010).

In chapter I and II, we investigated the dynamic changes in cellular architecture caused due to cytoskeleton-matrix interactions being affected by changes in matrix stresses. Our results revealed that stress fibers are much more sensitive to strain rate than strain frequency of applied stretch. Our results also indicated that cellular remodeling in response to stretch is exquisitely sensitive to the mechanical properties of the matrix. In summary, we present experimental evidence establishing a role for substrate stiffness and matrix stress in stretch induced cell alignment. We propose that active orientation of the actin cytoskeleton perpendicular and parallel to direction of stretch on stiff and soft

---

*Part of the chapter and the data in this chapter is reprinted from

"Dependence of cyclic stretch-induced stress fiber reorientation on stretch waveform." J Biomech 45(5): 728-735., Tondon, A., H. J. Hsu and R. Kaunas, Copyright (2012), with permission from Elsevier.

substrate, respectively, represents a mechanism by which cells stabilize the intracellular tension at an optimal level. Further, our results indicate that cells can align along directions of matrix stress without fibril alignment, indicating that matrix stress can directly regulate cell morphology.

ECM represents an essential player in stem cell niche, as it can directly or indirectly modulate the maintenance, proliferation, self-renewal and differentiation of stem cells. Several ECM molecules play regulatory functions for different types of stem cells, and based on its molecular composition ECM provides the most appropriate niche for stem cells in the tissue. ECM secreted by bone marrow cells, including fibronectin, laminin, collagens, has been shown to play an important roles in the maintenance of bone stem cells function, retention and osteogenic differentiation. Recently, Dr. Gregory's lab showed that a combination of hMSCs and their secreted anabolic extracellular matrix enhances repair of critical sized bone defects. They predicted that hMSC-derived collagens provides osteogenic retention signal for both exogenous hMSCs and host-derived cells (Zeitouni, Krause et al. 2012). In Chapter III, we demonstrated a novel method to covalently link hMatrix to PEEK surface, thus enhancing cellular adhesion and osteogenesis. PEEK surface does not naturally support cell adhesion and has to be modified to improve tissue integration. We predict that hMatrix coating on PEEK surface provides an anabolic bone microenvironment and will enhance repair and tissue integration of the PEEK implant.

In chapter IV, we utilized the unique conditions of simulated microgravity to develop a 3D model of bone stem cell-tumor interactions using hMatrix coated microsphere which

provide an excellent substratum for the support of osteogenic activity of bone stem cells. We expect the results from this study will lead to a range of new methods for the investigation of tumor-stem cell interactions without the limitations of 2D tissue culture or *in vivo* approaches. Furthermore, we expect that this approach will significantly accelerate drug research in this field and many other areas.

REFERENCES

Banes A,. J., M. Tsuzaki, J. Yamamoto, T. Fischer, B. Brigman, T. Brown and L. Miller (1995). "Mechanoreception at the cellular level: the detection, interpretation, and diversity of responses to mechanical signals." Biochem Cell Biol **73**(7-8): 349-365.

Barzegari, A. and A. A. Saei (2012). "An update to space biomedical research: tissue engineering in microgravity bioreactors." Bioimpacts **2**(1): 23-32.

Becker, M., S. Lorenz, D. Strand, C. F. Vahl and M. Gabriel (2013). "Covalent grafting of the RGD-peptide onto polyetheretherketone surfaces via Schiff base formation." Scientific World Journal: 616535.

Bellows, C. G., A. H. Melcher and J. E. Aubin (1982). "Association between tension and orientation of periodontal ligament fibroblasts and exogenous collagen fibres in collagen gels in vitro." J Cell Sci **58**: 125-138.

Boden, S. D. (2000). "Biology of lumbar spine fusion and use of bone graft substitutes: present, future, and next generation." Tissue Eng **6**(4): 383-399.

Briem, D., S. Strametz, K. Schroder, N. M. Meenen, W. Lehmann, W. Linhart, A. Ohl and J. M. Rueger (2005). "Response of primary fibroblasts and osteoblasts to plasma treated polyetheretherketone (PEEK) surfaces." J Mater Sci Mater Med **16**(7): 671-677.

Burger, J. A. and T. J. Kipps (2002). "Chemokine receptors and stromal cells in the homing and homeostasis of chronic lymphocytic leukemia B cells." Leuk Lymphoma **43**(3): 461-466.

Burridge, K., K. Fath, T. Kelly, G. Nuckolls and C. Turner (1988). "Focal adhesions: transmembrane junctions between the extracellular matrix and the cytoskeleton." Annu Rev Cell Biol **4**: 487-525.

Campbell, J. P., A. R. Merkel, S. K. Masood-Campbell, F. Elefteriou and J. A. Sterling (2012). "Models of bone metastasis." J Vis Exp(67): e4260.

Cappadona, C., E. M. Redmond, N. G. Theodorakis, I. H. McKillop, R. Hendrickson, A. Chhabra, J. V. Sitzmann and P. A. Cahill (1999). "Phenotype dictates the growth response of vascular smooth muscle cells to pulse pressure in vitro." Exp Cell Res **250**(1): 174-186.

Choidas, A., A. Jungbluth, A. Sechi, J. Murphy, A. Ullrich and G. Marriott (1998). "The suitability and application of a GFP-actin fusion protein for long-term imaging of the

organization and dynamics of the cytoskeleton in mammalian cells." Eur J Cell Biol **77**(2): 81-90.
Costa, K. D., W. J. Hucker and F. C. Yin (2002). "Buckling of actin stress fibers: a new wrinkle in the cytoskeletal tapestry." Cell Motil Cytoskeleton **52**(4): 266-274.

Dartsch, P. C. and E. Betz (1989). "Response of cultured endothelial cells to mechanical stimulation." Basic Res Cardiol **84**(3): 268-281.

Davies, P. F. and S. C. Tripathi (1993). "Mechanical stress mechanisms and the cell. An endothelial paradigm." Circ Res **72**(2): 239-245.

De, R., A. Zemel and S. A. Safran (2007). "Dynamics of Cell Orientation." Nature Physics **3**: 655-659.

Deibler, M., J. P. Spatz and R. Kemkemer (2011). "Actin fusion proteins alter the dynamics of mechanically induced cytoskeleton rearrangement." PLoS One **6**(8): e22941.

Deshpande, V. S., R. M. McMeeking and A. G. Evans (2006). "A bio-chemo-mechanical model for cell contractility." Proc Natl Acad Sci U S A **103**(38): 14015-14020.

Engler, A., L. Bacakova, C. Newman, A. Hategan, M. Griffin and D. Discher (2004). "Substrate compliance versus ligand density in cell on gel responses." Biophys J **86**(1 Pt 1): 617-628.

Engler, A. J., S. Sen, H. L. Sweeney and D. E. Discher (2006). "Matrix elasticity directs stem cell lineage specification." Cell **126**(4): 677-689.

Fouchard, J., D. Mitrossilis and A. Asnacios (2011). "Acto-myosin based response to stiffness and rigidity sensing." Cell Adh Migr **5**(1): 16-19.

Freed, L. E., R. Langer, I. Martin, N. R. Pellis and G. Vunjak-Novakovic (1997). "Tissue engineering of cartilage in space." Proc Natl Acad Sci U S A **94**(25): 13885-13890.

Fung, Y. C. (1994). "A First Course in Continuum Mechanics for Physical and Biological Engineers and Scientists." Prentice-hall.

Galbraith, C. G. and M. P. Sheetz (1998). "Forces on adhesive contacts affect cell function." Curr Opin Cell Biol **10**(5): 566-571.

Gavara, N., P. Roca-Cusachs, R. Sunyer, R. Farre and D. Navajas (2008). "Mapping cell-matrix stresses during stretch reveals inelastic reorganization of the cytoskeleton." Biophys J **95**(1): 464-471.

Girton, T. S., V. H. Barocas and R. T. Tranquillo (2002). "Confined compression of a tissue-equivalent: collagen fibril and cell alignment in response to anisotropic strain." J Biomech Eng **124**(5): 568-575.

Glass, D. A., 2nd and G. Karsenty (2007). "In vivo analysis of Wnt signaling in bone." Endocrinology **148**(6): 2630-2634.

Goodwin, T. J., T. L. Prewett, D. A. Wolf and G. F. Spaulding (1993). "Reduced shear stress: a major component in the ability of mammalian tissues to form three-dimensional assemblies in simulated microgravity." J Cell Biochem **51**(3): 301-311.

Green, E., J. D. Lubahn and J. Evans (2005). "Risk factors, treatment, and outcomes associated with nonunion of the midshaft humerus fracture." J Surg Orthop Adv **14**(2): 64-72.

Gregory, C. A., W. G. Gunn, E. Reyes, A. J. Smolarz, J. Munoz, J. L. Spees and D. J. Prockop (2005). "How Wnt signaling affects bone repair by mesenchymal stem cells from the bone marrow." Ann N Y Acad Sci **1049**: 97-106.

Grimm, D., M. Wehland, J. Pietsch, G. Aleshcheva, P. Wise, J. van Loon, C. Ulbrich, N. E. Magnusson, M. Infanger and J. Bauer (2014). "Growing tissues in real and simulated microgravity: new methods for tissue engineering." Tissue Eng Part B Rev **20**(6): 555-566.

Grotewold, L. and U. Ruther (2002). "The Wnt antagonist Dickkopf-1 is regulated by Bmp signaling and c-Jun and modulates programmed cell death." EMBO J **21**(5): 966-975.

Guilak, F., D. M. Cohen, B. T. Estes, J. M. Gimble, W. Liedtke and C. S. Chen (2009). "Control of stem cell fate by physical interactions with the extracellular matrix." Cell Stem Cell **5**(1): 17-26.

Hammond, T. G. and J. M. Hammond (2001). "Optimized suspension culture: the rotating-wall vessel." Am J Physiol Renal Physiol **281**(1): F12-25.

Hayakawa, K., N. Sato and T. Obinata (2001). "Dynamic reorientation of cultured cells and stress fibers under mechanical stress from periodic stretching." Exp Cell Res **268**(1): 104-114.

Hoffman, R. M. (1994). "The three-dimensional question: can clinically relevant tumor drug resistance be measured in vitro?" Cancer Metastasis Rev **13**(2): 169-173.

Hotulainen, P. and P. Lappalainen (2006). "Stress fibers are generated by two distinct actin assembly mechanisms in motile cells." J Cell Biol **173**(3): 383-394.

Hsu, H. J., C. F. Lee and R. Kaunas (2009). "A dynamic stochastic model of frequency-dependent stress fiber alignment induced by cyclic stretch." PLoS One **4**(3): e4853.

Hsu, H. J., C. F. Lee, A. Locke, S. Q. Vanderzyl and R. Kaunas (2010). "Stretch-induced stress fiber remodeling and the activations of JNK and ERK depend on mechanical strain rate, but not FAK." PLoS One **5**(8).

Hsu, H. J., C. F. Lee, A. Locke, S. Q. Vanderzyl and R. Kaunas (2010). "Stretch-induced stress fiber remodeling and the activations of JNK and ERK depend on mechanical strain rate, but not FAK." PLoS One **5**(8): e12470.

Jungbauer, S., H. Gao, J. P. Spatz and R. Kemkemer (2008). "Two characteristic regimes in frequency-dependent dynamic reorientation of fibroblasts on cyclically stretched substrates." Biophys J **95**(7): 3470-3478.

Kang, H., H. I. Kwak, R. Kaunas and K. J. Bayless (2011). "Fluid shear stress and sphingosine 1-phosphate activate calpain to promote membrane type 1 matrix metalloproteinase (MT1-MMP) membrane translocation and endothelial invasion into three-dimensional collagen matrices." J Biol Chem **286**(49): 42017-42026.

Kaspar, D., W. Seidl, C. Neidlinger-Wilke, A. Beck, L. Claes and A. Ignatius (2002). "Proliferation of human-derived osteoblast-like cells depends on the cycle number and frequency of uniaxial strain." J Biomech **35**(7): 873-880.

Katoh, K., Y. Kano, M. Amano, K. Kaibuchi and K. Fujiwara (2001). "Stress fiber organization regulated by MLCK and Rho-kinase in cultured human fibroblasts." Am J Physiol Cell Physiol **280**(6): C1669-1679.

Kaunas, R. and S. Deguchi (2011). "Sarcomeric model of stretch-induced stress fiber reorganization " Cell Health and Cytoskeleton **3** (1): 13-22

Kaunas, R., P. Nguyen, S. Usami and S. Chien (2005). "Cooperative effects of Rho and mechanical stretch on stress fiber organization." Proc Natl Acad Sci U S A **102**(44): 15895-15900.

Kaunas, R., S. Usami and S. Chien (2006). "Regulation of stretch-induced JNK activation by stress fiber orientation." Cell Signal **18**(11): 1924-1931.

Krause, U. and C. A. Gregory (2012). "Potential of modulating Wnt signaling pathway toward the development of bone anabolic agent." Curr Mol Pharmacol **5**(2): 164-173.

Krause, U., S. Harris, A. Green, J. Ylostalo, S. Zeitouni, N. Lee and C. A. Gregory (2010). "Pharmaceutical modulation of canonical Wnt signaling in multipotent stromal

cells for improved osteoinductive therapy." Proc Natl Acad Sci U S A **107**(9): 4147-4152.

Krause, U., D. M. Ryan, B. H. Clough and C. A. Gregory (2014). "An unexpected role for a Wnt-inhibitor: Dickkopf-1 triggers a novel cancer survival mechanism through modulation of aldehyde-dehydrogenase-1 activity." Cell Death Dis **5**: e1093.

Kretschmann, K. L. and A. L. Welm (2012). "Mouse models of breast cancer metastasis to bone." Cancer Metastasis Rev **31**(3-4): 579-583.

Krishnan, R., C. Y. Park, Y. C. Lin, J. Mead, R. T. Jaspers, X. Trepat, G. Lenormand, D. Tambe, A. V. Smolensky, A. H. Knoll, J. P. Butler and J. J. Fredberg (2009).

"Reinforcement versus fluidization in cytoskeletal mechanoresponsiveness." PLoS One **4**(5): e5486.

Kumar, S., I. Z. Maxwell, A. Heisterkamp, T. R. Polte, T. P. Lele, M. Salanga, E. Mazur and D. E. Ingber (2006). "Viscoelastic retraction of single living stress fibers and its impact on cell shape, cytoskeletal organization, and extracellular matrix mechanics." Biophys J **90**(10): 3762-3773.

Kurtz, S. M. and J. N. Devine (2007). "PEEK biomaterials in trauma, orthopedic, and spinal implants." Biomaterials **28**(32): 4845-4869.

Kwon, O., S. B. Devarakonda, J. M. Sankovic and R. K. Banerjee (2008). "Oxygen transport and consumption by suspended cells in microgravity: a multiphase analysis." Biotechnol Bioeng **99**(1): 99-107.

Lee, C. F., C. Haase, S. Deguchi and R. Kaunas (2010). "Cyclic stretch-induced stress fiber dynamics - dependence on strain rate, Rho-kinase and MLCK." Biochem Biophys Res Commun **401**(3): 344-349.

Lee, S. L., A. Nekouzadeh, B. Butler, K. M. Pryse, W. B. McConnaughey, A. C. Nathan, W. R. Legant, P. M. Schaefer, R. B. Pless, E. L. Elson and G. M. Genin (2012). "Physically-induced cytoskeleton remodeling of cells in three-dimensional culture." PLoS One **7**(12): e45512.

Macklis, J. D., R. L. Sidman and H. D. Shine (1985). "Cross-linked collagen surface for cell culture that is stable, uniform, and optically superior to conventional surfaces." In Vitro Cell Dev Biol **21**(3 Pt 1): 189-194.

Mardia, K. V. and P. Jupp (2000). Directional Statistics, John WIley and Sons Ltd.

Marsh, D. (1998). "Concepts of fracture union, delayed union, and nonunion." Clin Orthop Relat Res(355 Suppl): S22-30.

Matsui, T. S., S. Deguchi, N. Sakamoto, T. Ohashi and M. Sato (2009). "A versatile micro-mechanical tester for actin stress fibers isolated from cells." Biorheology **46**(5): 401-415.

Molloy, A. P., F. T. Martin, R. M. Dwyer, T. P. Griffin, M. Murphy, F. P. Barry, T. O'Brien and M. J. Kerin (2009). "Mesenchymal stem cell secretion of chemokines during differentiation into osteoblasts, and their potential role in mediating interactions with breast cancer cells." Int J Cancer **124**(2): 326-332.

Mukhopadhyay, M., S. Shtrom, C. Rodriguez-Esteban, L. Chen, T. Tsukui, L. Gomer, D. W. Dorward, A. Glinka, A. Grinberg, S. P. Huang, C. Niehrs, J. C. Izpisua Belmonte and H. Westphal (2001). "Dickkopf1 is required for embryonic head induction and limb morphogenesis in the mouse." Dev Cell **1**(3): 423-434.

Owen, J. D., P. J. Ruest, D. W. Fry and S. K. Hanks (1999). "Induced focal adhesion kinase (FAK) expression in FAK-null cells enhances cell spreading and migration requiring both auto- and activation loop phosphorylation sites and inhibits adhesion-dependent tyrosine phosphorylation of Pyk2." Mol Cell Biol **19**(7): 4806-4818.

Pang, Y., X. Wang, D. Lee and H. P. Greisler (2011). "Dynamic quantitative visualization of single cell alignment and migration and matrix remodeling in 3-D collagen hydrogels under mechanical force." Biomaterials **32**(15): 3776-3783.

Parameswaran, S. and R. S. Verma (2011). "Scanning electron microscopy preparation protocol for differentiated stem cells." Anal Biochem **416**(2): 186-190.

Pinzone, J. J., B. M. Hall, N. K. Thudi, M. Vonau, Y. W. Qiang, T. J. Rosol and J. D. Shaughnessy, Jr. (2009). "The role of Dickkopf-1 in bone development, homeostasis, and disease." Blood **113**(3): 517-525.

Plotnikov, S. V., A. M. Pasapera, B. Sabass and C. M. Waterman (2012). "Force Fluctuations within Focal Adhesions Mediate ECM-Rigidity Sensing to Guide Directed Cell Migration." Cell **151**(7): 1513-1527.

Ponten, J. and E. Saksela (1967). "Two established in vitro cell lines from human mesenchymal tumours." Int J Cancer **2**(5): 434-447.

Qiang, Y. W., Y. Chen, O. Stephens, N. Brown, B. Chen, J. Epstein, B. Barlogie and J. D. Shaughnessy, Jr. (2008). "Myeloma-derived Dickkopf-1 disrupts Wnt-regulated osteoprotegerin and RANKL production by osteoblasts: a potential mechanism underlying osteolytic bone lesions in multiple myeloma." Blood **112**(1): 196-207.

Reinhart-King, C. A. (2008). "Endothelial cell adhesion and migration." Methods Enzymol **443**: 45-64.

Reinhart-King, C. A., M. Dembo and D. A. Hammer (2008). "Cell-cell mechanical communication through compliant substrates." Biophys J **95**(12): 6044-6051.

Rihn, J. A., K. Kirkpatrick and T. J. Albert (2010). "Graft options in posterolateral and posterior interbody lumbar fusion." Spine (Phila Pa 1976) **35**(17): 1629-1639.

Roby, T., S. Olsen and J. Nagatomi (2008). "Effect of sustained tension on bladder smooth muscle cells in three-dimensional culture." Ann Biomed Eng **36**(10): 1744-1751.

Ronan, W., V. S. Deshpande, R. M. McMeeking and J. P. McGarry (2013). "Cellular contractility and substrate elasticity: a numerical investigation of the actin cytoskeleton and cell adhesion." Biomech Model Mechanobiol.

Roodman, G. D. (2004). "Mechanisms of bone metastasis." N Engl J Med **350**(16): 1655-1664.

Rose, A. A. and P. M. Siegel (2010). "Emerging therapeutic targets in breast cancer bone metastasis." Future Oncol **6**(1): 55-74.

Saez, A., M. Ghibaudo, A. Buguin, P. Silberzan and B. Ladoux (2007). "Rigidity-driven growth and migration of epithelial cells on microstructured anisotropic substrates." Proc Natl Acad Sci U S A **104**(20): 8281-8286.

Sato, K., T. Adachi, M. Matsuo and Y. Tomita (2005). "Quantitative evaluation of threshold fiber strain that induces reorganization of cytoskeletal actin fiber structure in osteoblastic cells." J Biomech **38**(9): 1895-1901.

Schwarz, U. S., T. Erdmann and I. B. Bischofs (2006). "Focal adhesions as mechanosensors: the two-spring model." Biosystems **83**(2-3): 225-232.

Takemasa, T., T. Yamaguchi, Y. Yamamoto, K. Sugimoto and K. Yamashita (1998). "Oblique alignment of stress fibers in cells reduces the mechanical stress in cyclically deforming fields." Eur J Cell Biol **77**(2): 91-99.

Tanner, K., A. Boudreau, M. J. Bissell and S. Kumar (2010). "Dissecting regional variations in stress fiber mechanics in living cells with laser nanosurgery." Biophys J **99**(9): 2775-2783.

Tian, E., F. Zhan, R. Walker, E. Rasmussen, Y. Ma, B. Barlogie and J. D. Shaughnessy, Jr. (2003). "The role of the Wnt-signaling antagonist DKK1 in the development of osteolytic lesions in multiple myeloma." N Engl J Med **349**(26): 2483-2494.

Todd, P. (1989). "Gravity-dependent phenomena at the scale of the single cell." ASGSB Bull **2**: 95-113.

Todd, P. (1991). "Gravity dependent processes and intracellular motion." ASGSB Bull **4**(2): 35-39.

Tondon, A., H. J. Hsu and R. Kaunas (2012). "Dependence of cyclic stretch-induced stress fiber reorientation on stretch waveform." J Biomech **45**(5): 728-735.

Tondon, A. and R. Kaunas (2014). "The direction of stretch-induced cell and stress fiber orientation depends on collagen matrix stress." PLoS One **9**(2): e89592.

Trepat, X., L. Deng, S. S. An, D. Navajas, D. J. Tschumperlin, W. T. Gerthoffer, J. P. Butler and J. J. Fredberg (2007). "Universal physical responses to stretch in the living cell." Nature **447**(7144): 592-595.

Trichet, L., J. Le Digabel, R. J. Hawkins, S. R. Vedula, M. Gupta, C. Ribrault, P. Hersen, R. Voituriez and B. Ladoux (2012). "Evidence of a large-scale mechanosensing mechanism for cellular adaptation to substrate stiffness." Proc Natl Acad Sci U S A **109**(18): 6933-6938.

Tsao, Y. D., T. J. Goodwin, D. A. Wolf and G. F. Spaulding (1992). "Responses of gravity level variations on the NASA/JSC bioreactor system." Physiologist **35**(1 Suppl): S49-50.

Unsworth, B. R. and P. I. Lelkes (1998). "Growing tissues in microgravity." Nat Med **4**(8): 901-907.

Urashima, M., B. P. Chen, S. Chen, G. S. Pinkus, R. T. Bronson, D. A. Dedera, Y. Hoshi, G. Teoh, A. Ogata, S. P. Treon, D. Chauhan and K. C. Anderson (1997). "The development of a model for the homing of multiple myeloma cells to human bone marrow." Blood **90**(2): 754-765.

Vader, D., A. Kabla, D. Weitz and L. Mahadevan (2009). "Strain-induced alignment in collagen gels." PLoS One **4**(6): e5902.

van der Horst, G. and G. van der Pluijm (2012). "Preclinical models that illuminate the bone metastasis cascade." Recent Results Cancer Res **192**: 1-31.

Wang, J. H., P. Goldschmidt-Clermont, J. Wille and F. C. Yin (2001). "Specificity of endothelial cell reorientation in response to cyclic mechanical stretching." J Biomech **34**(12): 1563-1572.

Wang, N., I. M. Tolic-Norrelykke, J. Chen, S. M. Mijailovich, J. P. Butler, J. J. Fredberg and D. Stamenovic (2002). "Cell prestress. I. Stiffness and prestress are closely associated in adherent contractile cells." Am J Physiol Cell Physiol **282**(3): C606-616.

Wang, N., J. D. Tytell and D. E. Ingber (2009). "Mechanotransduction at a distance: mechanically coupling the extracellular matrix with the nucleus." Nat Rev Mol Cell Biol **10**(1): 75-82.

Wang, R., J. Xu, L. Juliette, A. Castilleja, J. Love, S. Y. Sung, H. E. Zhau, T. J. Goodwin and L. W. Chung (2005). "Three-dimensional co-culture models to study prostate cancer growth, progression, and metastasis to bone." Semin Cancer Biol **15**(5): 353-364.

Wei, Z., V. S. Deshpande, R. M. McMeeking and A. G. Evans (2008). "Analysis and interpretation of stress fiber organization in cells subject to cyclic stretch." J Biomech Eng **130**(3): 031009.

Yeung, T., P. C. Georges, L. A. Flanagan, B. Marg, M. Ortiz, M. Funaki, N. Zahir, W. Ming, V. Weaver and P. A. Janmey (2005). "Effects of substrate stiffness on cell morphology, cytoskeletal structure, and adhesion." Cell Motil Cytoskeleton **60**(1): 24-34.

Zeitouni, S., U. Krause, B. H. Clough, H. Halderman, A. Falster, D. T. Blalock, C. D. Chaput, H. W. Sampson and C. A. Gregory (2012). "Human mesenchymal stem cell-derived matrices for enhanced osteoregeneration." Sci Transl Med **4**(132): 132ra155.

Zemel, A., F. Rehfeldt, A. E. Brown, D. E. Discher and S. A. Safran (2010). "Optimal matrix rigidity for stress fiber polarization in stem cells." Nat Phys **6**(6): 468-473.

Zhang, W., D. S. Choi, Y. H. Nguyen, J. Chang and L. Qin (2013). "Studying cancer stem cell dynamics on PDMS surfaces for microfluidics device design." Sci Rep **3**: 2332.

Zuzarte-Luis, V., J. A. Montero, J. Rodriguez-Leon, R. Merino, J. C. Rodriguez-Rey and J. M. Hurle (2004). "A new role for BMP5 during limb development acting through the synergic activation of Smad and MAPK pathways." Dev Biol **272**(1): 39-52.

APPENDIX A

DETAILED MATERIAL AND METHOD*

Cell culture

U2OS osteosarcoma cells (MarinPharm GmbH) were cultured in GIBCO DMEM (Invitrogen) supplemented with 10% fetal bovine serum, 2mM L-glutamine, 1mM sodium pyruvate and 1mM penicillin/streptomycin (Sigma) as described previously (Owen, Ruest et al. 1999, Kaunas, Usami et al. 2006). hMSCs isolated from bone marrow aspirates are held in a hMSC repository at Institute of Regenerative medicine, funded by the NIH (Dr. Carl Gregory is co-Investigator). General cell expansion was performed in accordance with our standard protocol (Zeitouni, Krause et al. 2012). In brief, cells were cultured in complete culture medium (CCM) consisting of alpha minimal essential medium (Invitrogen), 20% FBS (Hyclone and Altanta Biologicals), 2 mM glutamine, 100 U/ml penicillin, and 100 mg/ml streptomycin (Invitrogen). For each passage, cells were seeded at 100 cm-2. Cells are then recovered by trypsinization followed by cryopreservation in α-MEM containing 50% FBS and 5% DMSO. Cell cultures, stretch experiments and microgravity experiment using Rotating Wall Vessel Bioreactor (RWV) were performed in a humidified 5% CO_2 incubator at 37°C.

---

*Part of the appendix and the data in this appendix is reprinted from

"Dependence of cyclic stretch-induced stress fiber reorientation on stretch waveform." J Biomech 45(5): 728-735., Tondon, A., H. J. Hsu and R. Kaunas, Copyright (2012), with permission from Elsevier.

Collagen hydrogel preparation and stretching experiment

Silicone rubber stretch chambers (Strex, Japan) were modified to form a circular well (15 mm diameter) by adhering a silicone rubber sheet onto the chambers (Fig. B.1). The chambers were initially coated with collagen (4 μg/cm^2) by adding 100 μl of 0.3 mg/ml rat tail collagen type I (BD Biosciences) in the well and allowing the water to evaporate. The collagen gels (3 mg/ml) were formed within the collagen-coated wells as described previously (Kang, Kwak et al. 2011). Any gels that did not attached completely to the sides of the wells were not used in the experiments.

Cells were cultured either on surface-adsorbed collagen sheets or on the top surface of the collagen gels and subjected to cyclic stretch by stretching the chambers with two linear motors (Zaber, Canada) as described previously (Tondon, Hsu et al. 2012). The entire stretch apparatus was mounted on the stainless steel stage (Gibraltar) of a Nikon FN1 upright microscope housed in a custom-made acrylic enclosure maintained at 37°C using a heat gun (Omega) regulated by a temperature controller (Omega).

Three-point finite strain analysis

The strains fields produced by the device were determined by tracking the displacement of fiducial marks on the top surface of the hydrogel and the bottom surface of the silicone rubber sheet. The marks were produced with a permanent ink pen on the silicone rubber sheets and with red fluorescent beads (0.2 μm Fluospheres, Molecular Probes) mixed into the collagen gels prior to polymerization. Triads of marks in a focus plane in various sites on each surface were selected to compute the symmetric Lagrangian strain

tensor at each location. The finite strains in the longitudinal (E_1) and lateral directions (E_2) were computed from the E_{11} and E_{22} components of the strain tensor (Fung, 1994), respectively.

$$E_1 = \sqrt{1 + 2E_{11}} - 1 \quad (3A)$$

$$E_2 = \sqrt{1 + 2E_{22}} - 1 \quad (3B)$$

Quantification of SF organization

After stretching, cells were rinsed with PBS, fixed with 4% paraformaldehyde and stained with Texas Red-phalloidin (Molecular Probes) as described previously (Kaunas, Nguyen et al. 2005). Although the cells expressed GFP-actin, Alexa 488-phalloidin staining provided a stronger and longer-lasting signal for prolonged periods of imaging. Images were captured using a Nikon C1 laser scanning confocal head with a 60× water-dipping objective illuminated with a 40-mW Argon ion laser and green Helium Neon laser (Melles Griot). The images were later analyzed using a custom algorithm in MATLAB (the MathWorks, Natick, MA) to quantify the SF orientation distributions as previously described (Kaunas, Nguyen et al. 2005). The results from multiple cells (n = 90 cells per condition) were summarized as angular histograms. As described previously (Hsu et al., 2009), we computed the circular variance for each orientation distribution by vectorially summing the individual orientation vector components, normalizing the result by the total number of vectors (*N*) and subtracting the result from unity (Mardia and Jupp, 2000)

$$\text{Circular Variance} = 1 - \frac{1}{N}\sqrt{\left(\sum_{i=1}^{N} \sin 2\theta^i\right)^2 + \left(\sum_{i=1}^{N} \cos 2\theta^i\right)^2} \quad (4)$$

where θ^i is the angle of the *i*th SF relative to the stretch direction. The angles were doubled to account for the bidirectionality of axial vectors, i.e. $2\theta = 2(\theta + 180°)$. The values range from 0 to 1, corresponding to perfectly aligned and totally uniform distributions, respectively. For determining the circular variance of a population of cells, the distribution in SF orientations was computed by summing the distributions from individual cells, with the histogram from each cell normalized so that each cell contributed equally to the total distribution.

Cell alignment and shape analysis

The cell alignment angle, defined as the orientation of the major elliptic axis of an individual cell with respect to the stretch axis, was measured using the Particle Analysis tool in ImageJ (NIH). The distributions of orientations are presented as circular histograms to illustrate the orientation of cells relative to the stretch direction. The images of phalloidin stained cells were used to identify the cell outline since there was background signal in the cytosol.

Live microscopy

One hour before starting the experiment, the media in each stretch chamber was changed to Hyclone L-15 CO_2-independent media (Fisher Scientific). The stretch device was

mounted under the objective of the confocal microscope and cells were subjected to 10% cyclic stretch. Stretching was paused periodically in the unstretched position for ~30s to allow focusing and imaging of GFP-actin in an individual cell over time as described previously (Hsu, Lee et al. 2010, Lee, Haase et al. 2010).

hMatrix harvesting and crosslinking to spheres

hMatrix was harvested from OEhMSC monolayers cultured for 8 days in α-minimal-essential-media containing 20% fetal bovine serum, 50 μg/ml ascorbic acid, 5 mM β-glycerol phosphate and 10 μM GW9662. OEhMSC monolayers were washed in PBS and frozen at -80°C to disrupt cell membranes, thawed, and scraped from the culture plate. Recovered cells and matrix were pelleted by centrifugation and suspended in lysis buffer (0.1% Triton X100, 1 mM $MgCl_2$, 10 μg/ml DNAse I, 10 mg/ml RNAse A in PBS) with shaking at 60 rpm for 4h at 37°C and an additional 16h in the presence of 0.125% (v/v) trypsin. The remaining hMatrix was recovered by centrifugation and washed in distilled water and chloroform. Finally, hMatrix was rinsed in acetone and air-dried under sterile conditions. At time of use, the hMatrix was reconstituted in 2% (v/v) acetic acid at a concentration of 1 mg/ml. By this method, approximately 1 mg of material can be generated per cm2 of monolayer.

hMatrix was crosslinked to plasma treated Corning Enhanced microcarriers using a modified approach described previously (Macklis, Sidman et al. 1985). Sterile, ready-to-use Corning Enhanced microcarriers (16 mg) were reconstituted in 10 mL water medium to achieve a density of 5.5 cm2/mL according to manufacturer’s instructions.

Microcarriers were resuspended in an excess solution of 1-Ethyl-3-(3-dimethylaminopropyl)carbodiimide (EDAC) and harvested hMatrix and incubated for 3h on a shaker at room temperature. The microspheres were washed twice with PBS and air dried. The dried spheres were UV sterilized and washed with α-MEM before seeding cells.

ELISA

ELISA for OPG and DKK-1 were carried out by using nonbiotinylated polyclonal capture antibodies and biotinylated detection antibodies that were commercially acquired (R&D Systems and PromoKine) on Nunc Immunosorp coated 96-well plates (Fisher Lifesciences). The biotinylated capture antibodies were detected by using horseradish peroxidase-conjugated streptavidin and TMB substrate (Pierce).

Real-time quantitative RT-PCR

Total RNA (1 mg) was used to make complementary DNA (cDNA) (SuperScript III cDNA kit, Invitrogen). For quantitative RT-PCR, 0.5 mg of cDNA was amplified in a 25-ml reaction containing SYBR Green PCR master mix (Fast SYBR Green, Applied Biosystems) on an Applied Biosystems 7500 Fast Real-Time PCR System. Expression of osteogenic markers Col I, RunX2 and BMP2 was calculated using 2−DDCT method with housekeeping gene Human GAPDH as reference. Standard curve were generated for Human GAPDH and mouse GAPDH for cell number analysis.

Briefly, below are the steps involved in performing qRT-PCR on cell cultured in RWV (Fig. A.1):

1. Isolate Sample: The cell – sphere aggregates were extracted from the RWV co-culture and frozen at -80°C.
2. mRNA Isolation: Frozen cell – sphere aggregates were thawed in lyses buffer and mRNA extraction was performed using commercial mRNA extraction kit (High Pure RNA Isolation Kit, Roche).
3. cDNA library creation – cDNA library were created using oligo-(dt) primers using SuperScript® III kit (ThermoFisher).
4. Primer Design: Optimal primers were designed for both target genes and reference gene using OligoPerfect designer.
5. qRT-PCR assay: qRT-PCR was performed using SYBR green (Invitrogen). The assays were performed in 96 well PCR plate using Applied Biosystems 7500 Fast Real- Time PCR system.
6. Validate assay Efficiencies: The assay efficiencies were validated by comparing the slope of log phase of RT-PCR cycle for the genes. Only when the efficiencies of the target and normalizer assays are identical or very similar the comparative Ct (ddCt) method can be used.
7. Data analysis: qRT-PCR data was analyzed and Ct values were measured for each sample. We used Delta-Delta-Ct (ddCt) algorithm to determine relative gene expression of target markers gene in co-culture as compared to control
8. Expression of Osteogenic differentiation markers in RWV co-culture experiment performed in presence of MOSJ –DKK1 and MOSJ – pLenti cells was compared to that in control hMSCs culture. mRNA expression level in MOSJ –DKK1 and

MOSJ –pLenti co-culture were compared to expression level in hMSCs culture on the corresponding day. The relative expression of target markers were calculated using the following equation:

$$Ratio = \frac{2^{CT(Target\ Marker, Control\ hMSCs\ Culture) - CT(ref, Control\ hMSCs\ Culture)}}{2^{CT(Target\ Marker, Co-Culture) - CT(ref, Co-Culture)}} \quad (5)$$

where, “target marker” refers to osteogenic marker and “ref” refers to housekeeping gene GAPDH.. We calculated the relative expression at day 2, 4 and 8.

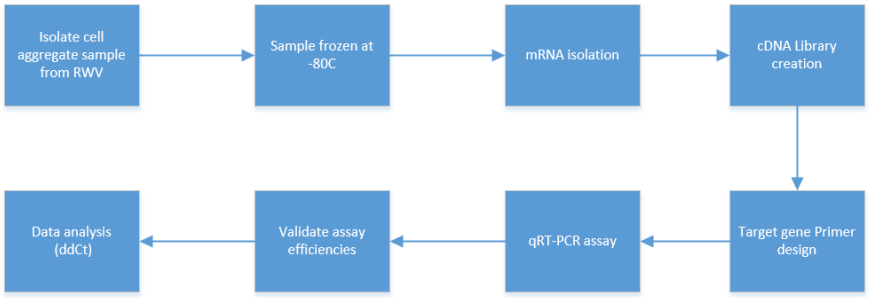

Figure A.1. Schematics of steps involved in qRT-PCR experiment from RWV culture.

Statistical analysis

The Rayleigh test was used to assess the degree of uniformity of distribution of axial vectors, i.e., whether the distribution has a significant direction. Average cos 2Θ values were calculated for each cell to obtain a distribution of values for each condition.

Significant differences between distributions were identified by ANOVA followed by Student-Newman–Keuls posthoc multiple comparisons testing.

APPENDIX B

SUPPLEMENTARY DATA

Figure B.1. Time-lapse images of a U2OS cell expressing GFP-actin subjected to 10% square-stretch at 0.01Hz over a period of 10.5h. Bar, 25 μm.

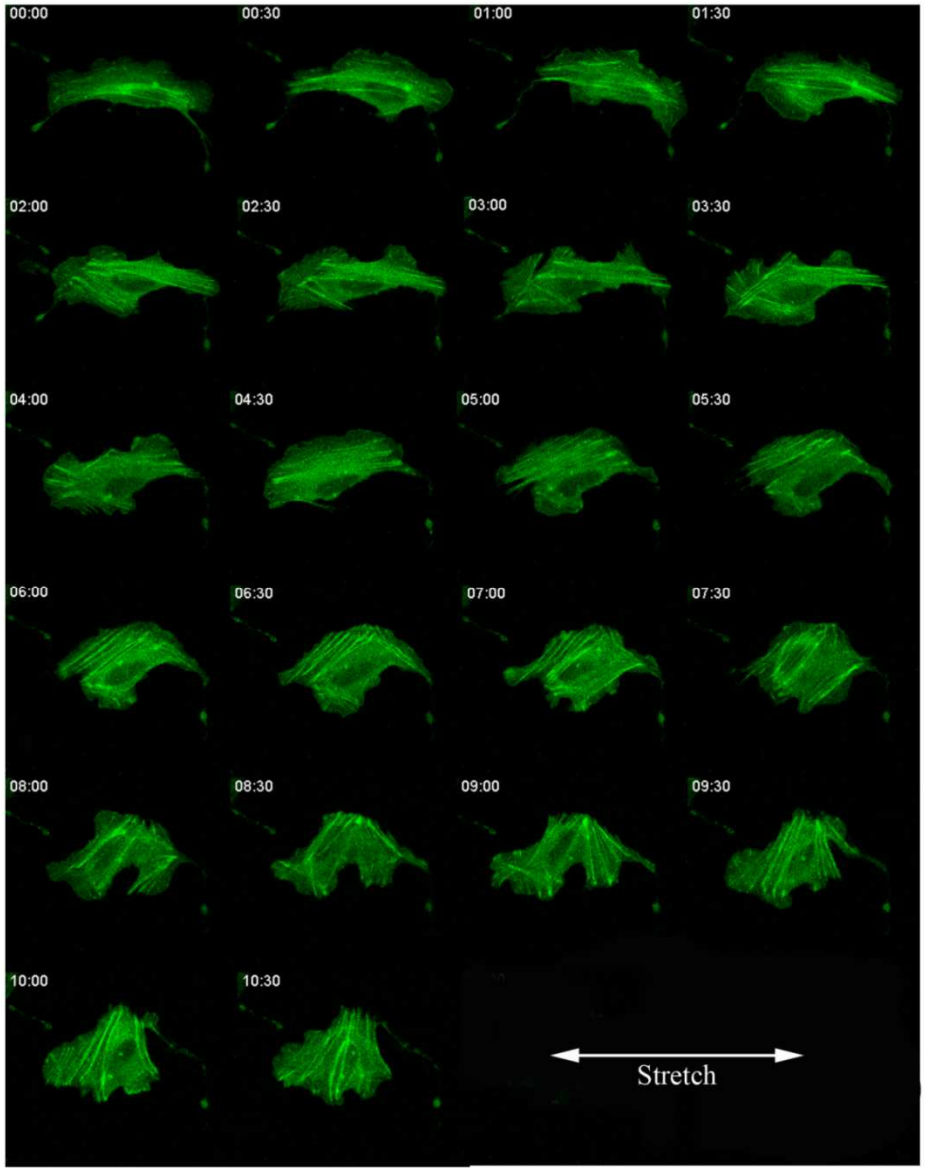

Figure B.2. Time-lapse images of a U2OS cell expressing GFP-actin subjected to subjected to 10% stretch at ramp rates of 20%/s. Imaging began immediately after the collagen hydrogel was stretched, with subsequent images captured at 10 min intervals for 2h. Scale bar, 5 μm.

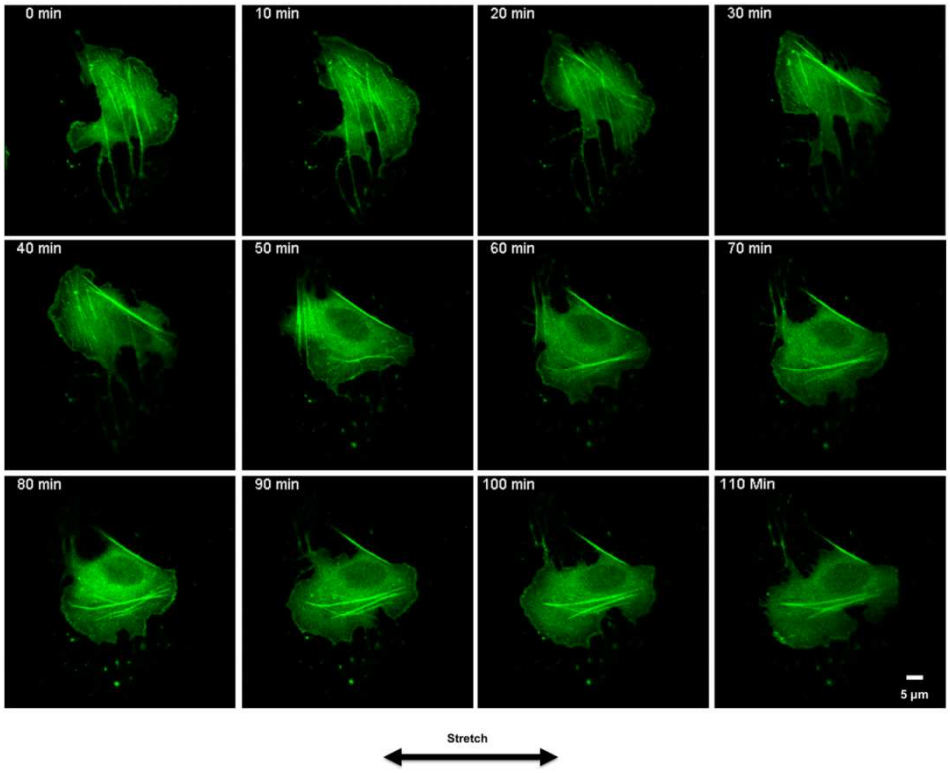

Figure B.3. Influence of substrate stiffness on cell elongation during stretch. Representative images of U2OS cells before and after a 10% step stretch depicting cell elongation and change in cell length in the direction of stretching for cells cultured on collagen gels (A) and collagen coated silicone rubber sheets (B) (n = 3). Reprinted from (Tondon and Kaunas 2014)

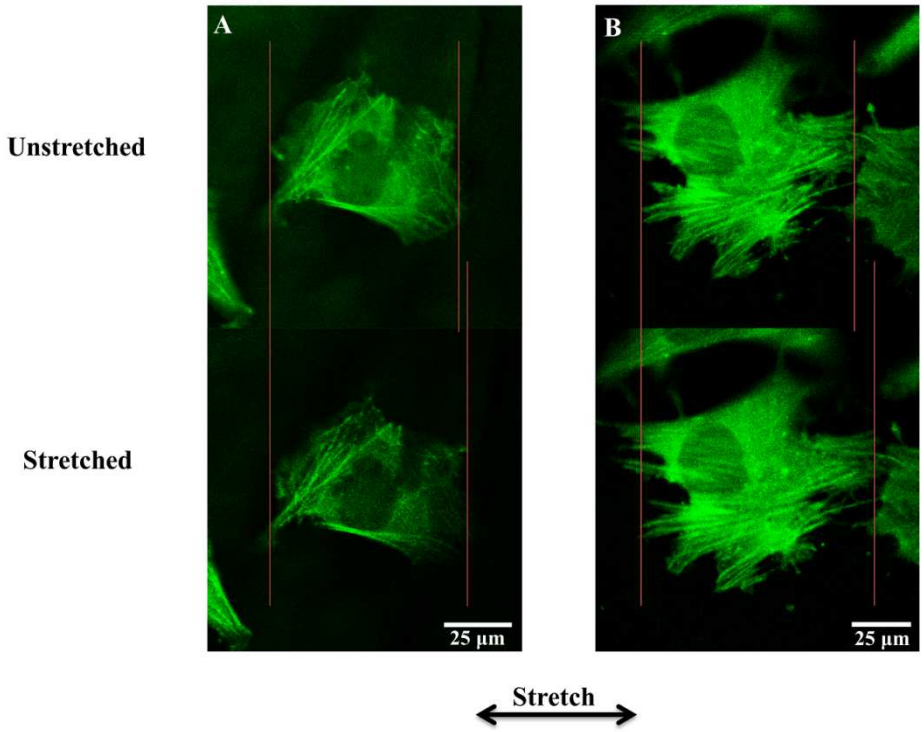

Table B.1. Influence of substrate stiffness on cell strains during stretch. Reprinted from (Tondon and Kaunas 2014)

		Applied Strain	**Longitudinal Strain**	**Lateral Strain**
Collagen	Substrate alone	0.1	0.093±0.009	-0.040±0.01
	Cell 1	0.1	0.063±0.01	-0.044±0.005
	Cell 2	0.1	0.058±0.014	-0.054±0.017
	Cell 3	0.1	0.061±0.008	-0.036±0.01
Silicone Rubber	Substrate alone	0.1	0.097±0.01	-0.041±0.005
	Cell 1	0.1	0.091±0.013	-0.046±0.004
	Cell 2	0.1	0.089±0.006	-0.027±0.008
	Cell 3	0.1	0.098±0.089	-0.024±0.004